Intense high-frequency laser-field control of spin-orbit coupling in GaInAs/AlInAs quantum wells: A laser dressing effect

Xue Li,[1,*] Wei Wang,[1,2,*] Ning Zhao,[1] Hao Yang,[1] Shixuan Han,[1] Wen Liu,[1,2] Hailong Wang,[1] Fanyao Qu,[3] Ning Hao,[4] Jiyong Fu,[1,3,†] and Ping Zhang[1,5,‡]

[1]*Department of Physics, Qufu Normal University, 273165 Qufu, Shandong, China*
[2]*Department of Physics, Jining University, 273155 Qufu, Shandong, China*
[3]*Instituto de Física, Universidade de Brasília, Brasília-DF 70919-970, Brazil*
[4]*Anhui Province Key Laboratory of Condensed Matter Physics at Extreme Conditions, High Magnetic Field Laboratory, HFIPS, Chinese Academy of Sciences, Hefei, 230031, China*
[5]*Beijing Computational Science Research Center, Beijing 100084, China*

(Received 6 June 2022; revised 6 October 2022; accepted 11 October 2022; published 21 October 2022)

The Rashba spin-orbit (SO) coupling can flexibly be controlled via an external gate, while the Dresselhaus term, which mainly depends on quantum confinement, is in general immune to electrical control. Here we theoretically report optical manipulation of the SO coupling by resorting to an intense high-frequency laser field, which "dresses" the confining potential for electrons as a result of optical stark effect and enables a flexible and simultaneous control of the Rashba and Dresselhaus couplings. Focusing on ordinary GaInAs/AlInAs quantum wells with two occupied subbands subject to both laser and gate fields, we perform a self-consistent Poisson-Schrödinger calculation in the Hartree approximation to determine *electro-optical* control of the intrasubband (intersubband) Rashba α_ν (η) and Dresselhaus β_ν (Γ) SO terms with $\nu = 1, 2$. Under the impact of laser field, we find that the Rashba terms of the two subbands α_1 and α_2 may remain locked to equal strength in a broad gate range, providing a means for *unified* manipulation of the two-subband Rashba couplings. Further, as the laser field varies, we observe that α_1 and α_2 may have either the same or opposite signs, or even α_2 vanishes while α_1 is finite, greatly fascinating for selective SO control of distinct subbands. For the Dresselhaus coupling, we disclose two distinct scenarios depending on the interplay of the well width and the laser field strength, and reveal that β_2 may decrease rapidly when the laser field strengthens, even though β_1 remains essentially constant. Regarding the intersubband Rashba (η) and Dresselhaus (Γ) terms, which mainly depend on the overlap and parity of the wave functions of the two subbands, they have relatively weak dependence on the laser field. Moreover, the combined effect of intra- and intersubband SO terms may lead to crossings and avoided crossings of the energy dispersion of multiband spin branches and may even trigger the spin polarization of an originally spin degenerate (unpolarized) band, tunable by the laser field. Our results should stimulate experiments probing the laser field mediated multiband SO control and further enables its spintronic applications.

DOI: 10.1103/PhysRevB.106.155420

I. INTRODUCTION

Spin orbit (SO) coupling, which arises from the relativistic Dirac equation, links the electron spin and spatial degrees of freedom, enabling coherent spin (magnetic moment) manipulation by purely electrical means [1–3]. Further, SO effects underlie various physical phenomena such as the SO torque [4,5], spin galvanic effect [6], topological insulators [7], Majorana fermions [8–10], and Weyl semimetals [11].

There are mainly two types of SO contributions in semiconductor heterostructures, i.e., the Rashba [12] and Dresselhaus [13] types, arising from the breaking of structural and crystal inversion symmetries, respectively. While conveniently facilitating coherent spin manipulation [1,3], the SO interaction also inherently causes spin relaxation [14,15]. A unique situation, i.e., persistent spin helix (PSH) [16–20], arises when the Rashba and Dresselhaus SO fields are matched, strongly protecting spins from relaxation. Koralek *et al.* first observed a PSH via transient spin grating spectroscopy [18]; Walser *et al.* imaged PSH using time-resolved Kerr rotation [19]. Following these, the PSH has been exploited in many different forms, including the drifting PSH driven by an in-plane electric field [21–24], the spin relaxation anisotropy mediated by an external magnetic field [25–27], and the phase diagram of interacting PSH states [28]. Also, Kammermeier *et al.* determined PSH symmetry of general crystal orientation [29] and even addressed persistent spin textures and currents in nanowire-based quantum systems with wurtzite structures [30]. Yoshizumi *et al.* demonstrated gate-controlled switching between a PSH state and inverse PSH state [31]. Alidoust reported a beautiful proposal for probing a PSH state via the critical supercurrent and ψ_0 state in two-dimensional (2D) Josephson junctions [32] and further

*These authors contributed equally to this work.
†yongjf@qfnu.edu.cn
‡zhang_ping@iapcm.ac.cn

with collaborators revealed dominant cubic SO coupling and anomalous Josephson effect [33]. By combining theoretical simulation and experimental (magnetoconductance) measurements, we achieved continuous locking of the Rashba and Dresselhaus couplings to equal strengths, bringing about the concept of the *stretchable* PSH [34,35]. Our recent proposal on the persistent skyrmion lattice hosted in quantum wells with two subbands [36], which can be realized by fine tuning the SO strengths, also manifests the importance of SO effects in semiconductor nanostructures. For comprehensive reviews of the PSH, see Refs. [37,38].

For controlling PSH symmetry and various other spintronic applications (e.g., spin-field and spin-Hall effect transistors), it is essential to achieve flexible SO control. The Rashba coefficient is essentially proportional to the external electric field, and thus can be tuned with the doping profile or by using a gate voltage [39,40]. Flexible control of the Rashba coupling in quantum heterostructures of either single [18,19,25,41,42] or double [43–49] occupancy for electrons has been well established. Moreover, we recently considered a triple-well structure, which favors the triple electron occupancy, and unveiled intriguing SO control triggered by the band crossing and anticrossing as well as the charge transfer among distinct subwells [50]. In contrast to the Rashba coupling, the Dresselhaus term mainly depends on quantum confinement (e.g., well width) [18,51] and hence is in general immune to electrical manipulation [52]. Considering practical applications of SO effects in various spintronic devices, for which the Rashba and Dresselhaus terms usually coexist [24,53–55], it is highly desirable to accomplish independent and simultaneous tuning of the two types of SO couplings both in a broad range.

Here, we aim to achieve a flexible and full manipulation of both Rashba and Dresselhaus terms in semiconductor heterostructures. To this end, we theoretically determine the laser field mediated *electro-optical* control of SO terms by combining the electrical and optical means [Fig. 1(a)]. Specifically, we resort to intense high-frequency laser (IHFL) fields [56–60], which by virtue of the so-called dressing effect greatly alters the confining potential [61] and further the quantized energy levels (i.e., optical stark effect [62–64]) for electrons confined in quantum wells, facilitating flexible control of the Dresselhaus coupling. This is far beyond the means of manipulating the Dresselhaus term by varying the well width, which involves distinct quantum systems. Focusing on ordinary GaInAs/AlInAs quantum wells having two occupied subbands for electrons, subjected to both laser and gate fields, we solve the coupled Schrödinger and Poisson equations to calculate the self-consistent outcome about laser dressed potential in the Hartree approximation, and further determine electro-optical control of all the relevant two-subband SO couplings, including the intrasubband (intersubband) Rashba α_ν (η) and Dresselhaus β_ν (Γ) terms, with $\nu = 1, 2$.

With the mediation of laser field, we demonstrate the *continuous* locking of α_1 and α_2 to equal strength as the gate voltage varies. This enables *unified* electro-optical manipulation of the two-subband Rashba couplings. Further, by adjusting the laser fields, we observe that α_1 and α_2 may have either the same or opposite signs, or even α_2 vanishes while α_1 is finite, greatly fascinating for selective SO control of distinct subbands. In addition, for the Dresselhaus coupling,

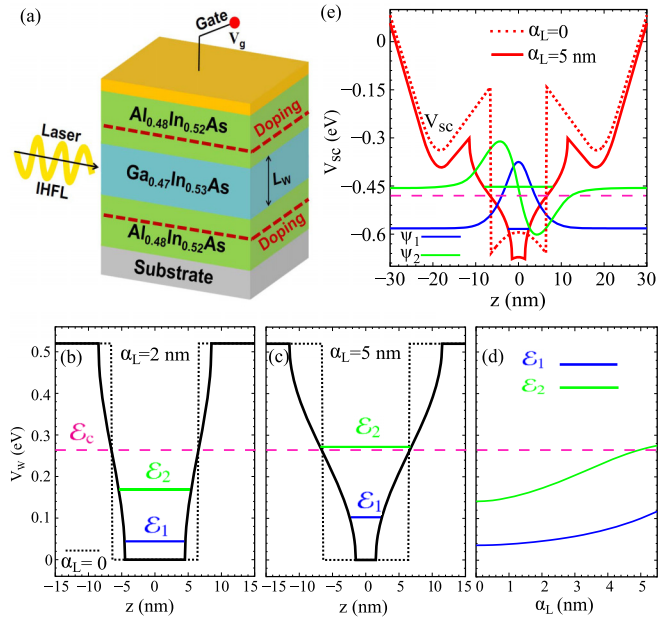

FIG. 1. (a) Schematic diagram of a $Ga_{0.47}In_{0.53}As/Al_{0.48}In_{0.52}As$ quantum well subject to the gate (V_g) and intense high-frequency laser (IHFL) fields, with L_w denoting the well width. The dashed (red) regions inside the barriers ($Al_{0.48}In_{0.52}As$) represent the doping layers with a symmetric doping condition. The polarization of laser field is in line with the well growth direction. (b), (c) Laser dressed structural potential (V_w) of the 13-nm well, manifesting two distinct scenarios for the change of *effective* well width seen by the two-subband electrons, with the energy levels $\mathcal{E}_1$ and $\mathcal{E}_2$ being both below $\mathcal{E}_c$ (b) and $\mathcal{E}_c$ sandwiched between $\mathcal{E}_1$ and $\mathcal{E}_2$ (c). The dotted (black) curve representing the structural potential in the absence of laser field (i.e., $\alpha_L = 0$) is shown alongside, for highlighting the laser dressing effect. The horizontal blue (green) line inside the well indicates the energy level $\mathcal{E}_1$ ($\mathcal{E}_2$) of the first (second) subband. (d) $\mathcal{E}_1$ and $\mathcal{E}_2$ versus the laser parameter α_L. In (b)–(d), the horizontal pink (dashed) line across the well refers to the critical energy $\mathcal{E}_c$, below (above) which the well width is effectively quenched (enlarged). (e) Total self-consistent potential V_{sc} and wave function profiles ψ_ν ($\nu = 1, 2$) for the 13-nm well at zero gate bias. The horizontal pink (dashed) line refers to the critical energy $\mathcal{E}_c^{sc}$ with self-consistence, an analog to $\mathcal{E}_c$ in (b)–(d) without self-consistence.

we disclose two distinct scenarios of SO control depending on the interplay of the well width and the laser field strength. We find that β_2 may decrease rapidly as the laser field strengthens, even though β_1 essentially remains constant. Regarding the intersubband Rashba (η) and Dresselhaus (Γ) SO terms, which mainly depend on the overlap and parity of the wave functions of the two subbands, we find that they have relatively weak dependence on laser field. Moreover, the combined effect of the intra- and intersubband SO terms may lead to crossings and avoided crossings of the energy dispersion of multiband spin branches and may even trigger the spin polarization of an originally spin degenerate (unpolarized) band, tunable by the laser field. Our results should stimulate experiments probing the laser field mediated multiband SO control and further enables its spintronic applications.

This paper is organized as follows. In Sec. II, we first present the laser dressed potential for quantum wells due to

the IHFL fields. Then, we derive an effective 2D Rashba and Dresselhaus SO Hamiltonian from a three-dimensional (3D) form for quantum wells with two occupied electron subbands. Further, we show the expressions of all the relevant intra- and intersubband SO interactions (both Rashba and Dresselhaus). The model system that we consider is introduced in Sec. III. In Sec. IV, we present our self-consistent results and discussion about the laser dressing effect mediated electro-optical SO control. We summarize our main findings in Sec. V.

II. THEORETICAL FRAMEWORK

Here we first outline the dressing effect of the IHFL field on the confining potential for electrons residing in quantum wells. Then, we present the derivation process of transforming the electron Hamiltonian from a 3D form to an effective 2D form. The relevant expressions of the Rashba and Dresselhaus SO terms of both intra- and intersubband kinds are also presented.

A. Laser dressed potential energy

The ultrashort (femtosecond to attosecond) laser pulses have enabled the generation of an intense light field, whose magnitude can even far exceed that of the atomic Coulomb field [65,66]. Thus, light, which had long been used only as a probe for matter, has now achieved such huge intensity that the electronic states bound in atoms, molecules, clusters, and solids could be strongly modified, namely the laser dressed electronic states (or potentials) [65–70]. We adopt a similar approach that has been developed to describe atomic behavior under the impact of IHFL fields. Specifically, in the dipole approximation, we consider that the radiation field, which is assumed linearly polarized, is represented by a monochromatic plane wave of angular frequency ω. With this consideration, the electrodynamic potential of the wave reads $\mathrm{A}(t) = A_0\cos(\omega t)\mathbf{e_P}$, with A_0 the potential amplitude and $\mathbf{e_P}$ the unit vector pointing along the polarization direction. By applying the Kramers-Henneberger space translation transformation to the Schrödinger equation, one obtains [56,57,71–74]

$$-\frac{\hbar^2}{2m^*}\nabla^2\psi(\mathbf{r},t) + V(\mathbf{r}+\alpha(t))\psi(\mathbf{r},t) = i\hbar\frac{\partial\psi(\mathbf{r},t)}{\partial t}, \quad (1)$$

where m^* is the effective electron mass and $\alpha(t) = \alpha_{\mathrm{L}}\sin(\omega t)\mathbf{e_P}$ stands for the quiver motion of electrons subjected to the laser field. Here $\alpha_{\mathrm{L}} = eA_0/m^*c\omega$ denotes the laser parameter and $V(\mathbf{r}+\alpha(t))$ represents the laser dressed potential energy, with e the electric charge and c the light speed. In terms of the time-averaged intensity I of the laser field, we rewrite the laser parameter α_{L}:

$$\alpha_{\mathrm{L}} = (I^{1/2}/\omega^2)(e/m^*)(8\pi/c)^{1/2}. \quad (2)$$

Following the Floquet approach [65], the space translated version of the Schrödinger equation [Eq. (1)] can be transformed into coupled time-independent differential equations in terms of the Floquet component of the wave function ψ, for which a Floquet state is the analog to a Bloch state when replacing a spatially periodic potential to a time-periodic one. To solve the resulting coupled differential equations, an iteration scheme, which essentially proceeds in inverse powers of ω, can be utilized. To the lowest order in ω, i.e., in the high-frequency limit, the set of coupled equations reduces to a single one [65,74,75],

$$\left(-\frac{\hbar^2}{2m^*}\nabla^2 + V(\mathbf{r};\alpha_{\mathrm{L}})\right)\psi_0 = E\psi_0, \quad (3)$$

with ψ_0 the zeroth Floquet component and $V(\mathbf{r};\alpha_{\mathrm{L}})$ the dressed confinement potential depending on ω and I through α_{L}.

Regarding ordinary quantum wells grown along the $z||(001)$ direction under the IHFL field, for which the polarization orientation is set in line with the growth direction of the well [Fig. 1(a)], the confining square potential seen by electrons, i.e., $V_{\mathrm{w}}^0(z) = \delta_c[\Theta(z - L_{\mathrm{w}}/2) + \Theta(-z - L_{\mathrm{w}}/2)]$, arising from the band offset at the interfaces, is corrected by the laser dressed one ($V_{\mathrm{w}}^0(z) \to V_{\mathrm{w}}(z;\alpha_{\mathrm{L}})$) [61,76], with

$$V_{\mathrm{w}}(z;\alpha_{\mathrm{L}}) = \frac{\delta_c}{\pi}\Bigg[\Theta(\alpha_{\mathrm{L}} - L_{\mathrm{w}}/2 - z)\arccos\left(\frac{L_{\mathrm{w}}/2+z}{\alpha_{\mathrm{L}}}\right) + \Theta(\alpha_{\mathrm{L}} - L_{\mathrm{w}}/2 + z)\arccos\left(\frac{L_{\mathrm{w}}/2-z}{\alpha_{\mathrm{L}}}\right)\Bigg]. \quad (4)$$

Here we have defined δ_c the conduction band offset, Θ the Heaviside function and L_{w} the well width. Clearly, in the limit of the laser parameter α_{L} approaching zero, V_{w} recovers the original square well potential (i.e., V_{w}^0).

So far, the laser dressing effect with IHFL field has exhibited strong experimental evidence and has been widely adopted in various experiments and applications, e.g., atomic stabilization [67], molecular dissociation [68], higher-order harmonic generation [77], and control of electronic and optical properties in semiconductor heterostructures [69,78,79], justifying our proposed approach for SO control is experimentally attainable.

B. SO Hamiltonians: From 3D to 2D

We consider GaInAs/AlInAs quantum wells grown along the $z\|(001)$ direction. Based on the 8×8 Kane model involving conduction and valence bands, an effective 3D Hamiltonian only for conducting electrons is obtained through the folding-down procedure [80,81],

$$\mathcal{H}^{3\mathrm{D}} = \frac{\hbar^2k^2}{2m^*} - \frac{\hbar^2}{2m^*}\frac{\partial^2}{\partial z^2} + V_{\mathrm{sc}}(z) + \mathcal{H}_R^{3\mathrm{D}} + \mathcal{H}_D^{3\mathrm{D}}, \quad (5)$$

where m^* is the effective mass of the electron and k is the in-plane electron momentum. The third term $V_{\mathrm{sc}} = V_{\mathrm{w}} + V_{\mathrm{g}} + V_{\mathrm{d}} + V_{\mathrm{e}}$ refers to the total electron confining potential, which is determined self-consistently by solving the Schrödinger and Poisson equations in the Hartree approximation. Here V_{w} is the structural potential arising from the band offset but with the laser dressing effect being accounted for [Eq. (4)], V_{g} refers to the contribution from the external gate potential, V_{d} denotes the modulation doping potential, and V_{e} stands for the purely electronic Hartree potential [34,36,49,81]. The last two terms $\mathcal{H}_R^{3\mathrm{D}}$ and $\mathcal{H}_D^{3\mathrm{D}}$ correspond to Rashba and Dresselhaus SO interactions, respectively. The Rashba term reads $\mathcal{H}_R^{3\mathrm{D}} = \eta(z)(k_x\sigma_y - k_y\sigma_x)$, where $\eta(z) = \eta_{\mathrm{w}}\partial_z V_{\mathrm{w}} + \eta_{\mathrm{H}}\partial_z(V_{\mathrm{g}} + V_{\mathrm{d}} +$

V_e) determines the Rashba coupling strength and $\sigma_{x,y,z}$ are the spin Pauli matrices. The parameters η_w and η_H are related to the bulk quantities of materials [49,81,82]. The Dresselhaus term has the form $\mathcal{H}_D^{3D} = \gamma[\sigma_x k_x(k_y^2 - k_z^2) + \text{c.p.})]$ with γ the bulk Dresselhaus parameter and $k_z = -i\partial_z$ [13,80].

Now we are ready to derive an effective 2D model starting from the 3D Hamiltonian [Eq. (5)]. For this purpose, we first determine (self-consistently) the spin-degenerate eigenstates of the quantum well in the *absence* of SO interaction $|\mathbf{k}\nu\sigma\rangle = |\mathbf{k}\nu\rangle \otimes |\sigma\rangle$, $\langle \mathbf{r}|\mathbf{k}\nu\rangle = \exp(i\mathbf{k}\cdot\mathbf{r})\psi_\nu(z)$ and the spin-degenerate eigenvalues $\varepsilon_{\mathbf{k}\nu} = \mathcal{E}_\nu + \hbar^2 k^2/2m^*$, with $\nu = 1, 2$. Here, $\mathcal{E}_\nu$ (ψ_ν) is defined as the νth quantized energy level (wave function), $\mathbf{k}$ the in-plane wave vector, and $\sigma = (\uparrow, \downarrow)$ the electron spin component along the z direction. Then, by projecting Eq. (5) with SO onto the spin-degenerate basis set $\{|\mathbf{k}\nu\sigma\rangle\}$, we can obtain the effective 2D form of the Rashba and Dresselhaus SO Hamiltonian with both intra- and intersuband terms for quantum wells of double electron occupancy. Specifically, under the coordinate system [$x\|(100)$, $y\|(010)$] with the basis set ordered by $\{|\mathbf{k}1\uparrow\rangle, |\mathbf{k}1\downarrow\rangle, |\mathbf{k}2\uparrow\rangle, |\mathbf{k}2\downarrow\rangle\}$, our effective 2D model with two subbands reads

$$\mathcal{H}^{2D} = \begin{pmatrix} \rho_{11} & \rho_{12} \\ \rho_{21} & \rho_{22} \end{pmatrix}, \tag{6}$$

where $\rho_{\nu\nu} = \varepsilon_{\mathbf{k}\nu}\mathbb{1} + \alpha_\nu(\sigma_y k_x - \sigma_x k_y) + \beta_\nu(\sigma_y k_y - \sigma_x k_x)$, $\nu = 1, 2$, $\rho_{12} = \eta(\sigma_y k_x - \sigma_x k_y) + \Gamma(\sigma_y k_y - \sigma_x k_x)$ and $\rho_{21} = \rho_{12}^\dagger$, with $\mathbb{1}$ the 2×2 matrix in both spin and orbital (subband) subspaces, $\sigma_{x,y}$ the spin Pauli matrices, $k_{x,y}$ the wave vector components along the $x\|(100)$ and $y\|(010)$ directions, and the parameters α_ν (η) and β_ν (Γ) represent intrasubband (intersubband) Rahsba and Dresselhaus SO coefficients, as we specify below.

Note that the effective 2D SO Hamiltonian [Eq. (6)] is written in the basis set of the two subbands (with spin), with $\nu = 1, 2$ the subband indices. Thus, the diagonal elements (ρ_{11} and ρ_{22}) are the intrasubband terms belonging to the subbands 1 and 2, and the off-diagonal terms (ρ_{12} and ρ_{21}) refer to the intersubband SO terms connecting (coupling) the two subbands. Also, for either the intra- or intersubband SO terms, both Rashba and Dresselhaus couplings are included. Further, all the SO terms belong to the *overall* well, rather than to a *local* region of the system, as they are determined by the self-consistent potential and wave functions of the whole system, below see Eqs. (7) and (8). For more details on how to derive Eq. (6) from Eq. (5), see the Supplemental Material (SM) [83].

Further, we should emphasize that the quantum tunneling effect has been *intrinsically* (*implicitly*) taken into account in our self-consistent calculation, since we solve the Schrödinger equation of the whole system comprising both the well and barrier layers. Thus, our approach is valid for various kinds of quantum wells; see also our recent works about single wells [81], double wells [36], and even multiple wells [50]. The key is that we solve the Schrödinger equation in a rigorous way, i.e., for the *overall* system, instead of just considering the scattering problem from a *local* barrier. And, for realistic considerations, the confining potential for electrons includes not only the structural potential V_w but also the doping potential V_d, the electron Hartree potential V_e and the external gate potential V_g.

C. Rashba and Dresselhaus SO coefficients

The Rashba SO coefficients appearing in Eq. (6) can be expressed as the matrix elements $\langle\cdots\rangle$ of the weighted derivatives of the potential contributions,

$$\eta_{\nu\nu'} = \langle\psi_\nu|\eta_w\partial_z V_w + \eta_H\partial_z(V_g + V_d + V_e)|\psi_{\nu'}\rangle, \tag{7}$$

and the Dresselhaus SO coefficients read

$$\Gamma_{\nu\nu'} = \gamma\langle\psi_\nu|k_z^2|\psi_{\nu'}\rangle, \tag{8}$$

with the intrasubband (intersubband) Rashba coefficients $\alpha_\nu \equiv \eta_{\nu\nu}$ ($\eta \equiv \eta_{12}$) and the Dresselhaus coefficients $\beta_\nu \equiv \Gamma_{\nu\nu}$ ($\Gamma \equiv \Gamma_{12}$). Here we have defined the intrasubband Rashba term α_ν as the sum of several constituent contributions, i.e., $\alpha_\nu = \alpha_\nu^g + \alpha_\nu^d + \alpha_\nu^e + \alpha_\nu^w$, with $\alpha_\nu^g = \eta_H\langle\psi_\nu|\partial_z V_g|\psi_\nu\rangle$ being the gate contribution, $\alpha_\nu^d = \eta_H\langle\psi_\nu|\partial_z V_d|\psi_\nu\rangle$ the doping contribution, $\alpha_\nu^e = \eta_H\langle\psi_\nu|\partial_z V_e|\psi_\nu\rangle$ the electron Hartree contribution, and $\alpha_\nu^w = \eta_w\langle\psi_\nu|\partial_z V_w|\psi_\nu\rangle$ the structural (plus laser-field) contribution. Note that here α_ν^w is beyond the usual structural term, as it contains contributions not only from the structural profile of a square well (interface effect) but also from the laser field (dressing effect) following from V_w representing the laser dressed potential [Eq. (4)]. Similarly, the intersubband Rashba term is written as $\eta = \eta^g + \eta^d + \eta^e + \eta^w$, while with η^j (j = g, d, e, w) being the matrix elements between different subbands (cf. η^j and α_ν^j). For convenience, we also use $\alpha_\nu^{g+d} = \alpha_\nu^g + \alpha_\nu^d$ and $\eta^{g+d} = \eta^g + \eta^d$.

For realistic wells, both the Rashba (α_ν) and Dresselhaus (β_ν) couplings only *implicitly* depend on the gate potential V_g (and the laser parameter α_L). In other words, these SO terms not only depend on V_g (and α_L) but also on the doping potential V_d, the electron Hartree potential V_e, and the laser dressed structural potential V_w. Therefore, for each value of V_g (and α_L), one has to self-consistently (numerically) determine the total confining potential $V_{sc} = V_w + V_g + V_d + V_e$ and the eigenenergy (and wave functions) of the system, and further the relevant SO coefficients [Eqs. (7) and (8)].

Despite the numerical restraint, one can still rewrite the Rashba coefficients in a more physical way for functional form by introducing an *effective* force field, $F_{\text{eff}}^\nu = F_{\text{gate}}^\nu + F_e^\nu + F_d^\nu$, in which $F_{\text{gate}}^\nu = -\langle\partial_z V_g\rangle_\nu$, $F_d^\nu = -\langle\partial_z V_d\rangle_\nu$, and $F_e^\nu = -\langle\partial_z V_e\rangle_\nu$. Specifically, since the total force on bound states is zero (Ehrenfest's theorem) [80], i.e., $\langle\partial_z V_{sc}\rangle_\nu = \langle\partial_z(V_w + V_g + V_d + V_e)\rangle_\nu = 0$, the Rashba coefficients in terms of the bulk Rashba parameters η_H and η_w [81,84] and the effective force field can be rewritten as

$$\alpha_\nu = (\eta_w - \eta_H)F_{\text{eff}}^\nu. \tag{9}$$

In particular, we turn to the change of α_ν due to a variation of F_{eff}^ν, e.g., a variation of V_g, giving rise to $\delta\alpha_\nu = (\eta_w - \eta_H)(\delta F_{\text{gate}}^\nu + \delta F_e^\nu + \delta F_d^\nu)$. In our model, the variation of $\delta F_d^\nu \simeq 0$ since the doping potential does not vary with both the gate and laser field. Also, in a special case of constant electron density [85], δF_e^ν is expected to be small [86] since the rearrangement of the quantum mechanical distributions of electrons may be negligible. With these particular considerations, we have $\delta\alpha_\nu \simeq (\eta_H - \eta_w)\delta F_{\text{gate}}^\nu$, depending on external gate fields. Similar treatment can be used for determining the dependence of α_ν on α_L, the effect of which is contained in the laser dressed potential [Eq. (4)]. Regarding

the Dresselhaus coefficents β_ν [Eq. (8)], with the help of the Schrödinger equation, it is straightforward to rewrite $\beta_\nu = \gamma(2m^*/\hbar^2)[\mathcal{E}_\nu - \langle V_{\rm sc}(z)\rangle_\nu]$, with $\mathcal{E}_\nu$ the νth subband energy level.

In addition, for better understanding the effective 2D SO model that we construct, in the SM we show a schematic with both spin and subband degrees of freedom (Fig. S4), *pictorially* illustrating all the relevant SO terms, of the intrasubband (α_ν and β_ν, within each subband) and intersuband (η and Γ, connecting the two subands) SO terms with both Rashba and Dresslehaus couplings.

III. SYSTEM AND PARAMETERS

We focus on ordinary (001)-grown $Ga_{0.47}In_{0.53}As$ quantum wells of width $L_{\rm w}$ sandwiched between $Al_{0.48}In_{0.52}As$ barriers [Fig. 1(a)], similar to the experimental sample of Refs. [81,87,88]. The structure is subjected to both the external gate bias ($V_{\rm g}$) and the IHFL field, allowing for combined (electro-optical) control of the SO coupling by electrical and optical means. The ionized dopants of width 6 nm in $Al_{0.48}In_{0.52}As$ barrier layers sit 10 nm away from either side of the well with the same doping density $\rho = 8\times10^{18}$ cm^{-3}, ensuring symmetric doping condition. The band offset at the $Ga_{0.47}In_{0.53}As/Al_{0.48}In_{0.52}As$ interfaces is set as $\delta_c = 0.52$ eV [49,89]. The temperature is 0.3 K. Note that the effect of temperature in the self-consistent procedure mainly enters the Fermi-Dirac distribution [34,49,81], which favors the occupation of higher-energy subbands at elevated temperatures. Thus, our results are essentially also valid for temperatures above 0.3 K within a regime that the higher third subband remains unoccupied.

We consider both a relatively narrow well and a relatively wide well, of the width of $L_{\rm w} = 13$ and 20 nm (unless stated otherwise in Sec. IV E), respectively, for covering a more complete picture of the laser dressing effect mediated SO control. The Fermi level $E_{\rm F}$, with which one can adjust the subband occupations, is pinned at a constant for a given quantum well to determine our self-consistent outcome [34,90], and the gate bias $V_{\rm g}$ is utilized for a simultaneous tuning of the electron occupancy and the structural inversion asymmetry (SIA) of the system. Further, by means of the laser field, which dresses the confining potential for electrons hosted in quantum wells, one can alter the extent of quantum confinement. For the two widths of wells, all the relevant parameters are the same except for the Fermi level, which determines the areal electron density. In order to make our system sustain the condition of double electron occupancy in the whole range of gate and laser fields considered, we set the Fermi level $E_{\rm F} = -0.45$ and -0.40 eV for the well of width $L_{\rm w} = 13$ and 20 nm, respectively. Note that the Fermi level is readily tunable in experiments, e.g., via electrical means [91,92].

Referring to the IHFL field, the effect of which depends on both the laser intensity I and its frequency ω of oscillation. For quantum wells exposed to laser field, the high-frequency regime, in general, means that the condition of $\omega\tau \gg 1$ satisfies [93], where $\tau \sim$ ps denotes the transit time of electrons, so the electron could *see* an evident effect of the laser dressed potential. The frequency in such a regime could range from several to even thousands of THz, depending on specific applications [94,95]. In contrast, in the low-frequency regime of $\omega\tau \ll 1$ (not the focus of this paper), the electron is too fast for the transit process to see the laser dressing effect [96]. We restrict ourselves to SO properties without optical transitions, and only consider a scenario that the laser is tuned to be off resonance with both intersubband (condution-conduction bands) and interband (conduction-valence bands) transitions [97].

Besides the laser frequency, for ensuring a pronounced laser effect, we also consider the intense-laser regime, in which the amplitude of the electron oscillation (i.e., laser parameter $\alpha_{\rm L}$) is of the same order of (or greater than) the characteristic size of the bound system, namely, the effective Bohr radius $\alpha_{\rm B}^* = \hbar^2\epsilon_r/m^*ke^2$ [57,98], with e the free electron charge, ϵ_r the relative dielectric constant, and m^* the effective electron mass. This directly yields $I \sim I_{\rm c} = m^{*2}\alpha_{\rm B}^{*2}\omega^4 c\epsilon_0\epsilon_r^{1/2}/2e^2$. For our GaInAs wells, $\alpha_{\rm B}^* = 14.5$ nm and $I_{\rm c} = 9\times10^{11}$ W/cm^2 at $\omega/2\pi = 100$ THz, for which the high-frequency dielectric constant of $\epsilon_r = 11.7$ and effective electron mass $m^* = 0.043m_0$ are considered [89,99,100]. Here the laser parameter range that we consider is $\alpha_{\rm L} = 0-7$ nm, corresponding to the maximum light intensity of about 2×10^{11} W/cm^2 [101], comparable to $I_{\rm c}$.

Note that both the high frequency of hundreds of THz and the intense field of about 10^{12} W/cm^2 are widely adopted in experiments [58,102–105]. Further, even a laser field with a huge light intensity of about 10^{22} W/cm^2 and high frequency of about 1000 THz has also been attainable in experiments [106,107]. All these justify the laser field range that we consider as well as our theoretical prediction being feasible for future experimental verifications.

With all these considerations, we are ready to discuss our self-consistent outcome and combined (electro-optical) control of SO couplings by gate and laser fields.

IV. RESULTS AND DISCUSSION

Below we discuss the laser field mediated electro-optical control of the SO couplings. To proceed in a systematic way, we first present our self-consistent outcome for quantum wells in the presence of IHFL field. Then, we discuss the cases of SO manipulation by purely electrical and optical means. Further, we dig into the combined impact of gate and laser fields on the Rashba and Dresselhaus SO terms.

A. Self-consistent outcome about laser dressed potential: *Effective* well width and band offset

Before performing the self-consistent calculation, we first look into how the laser field alters the pure structural potential $V_{\rm w}$ for electrons [Eq. (4)]. In Fig. 1(b), we show the structural potential for the 13-nm well in both cases of the laser parameter $\alpha_{\rm L} = 2$ nm (solid curve) and 0 (dotted curve), for highlighting the impact of the laser field. As expected, the IHFL field by virtue of the laser dressing effect, which varies the *effective* width of the well, greatly alters the potential profile. Specifically, there emerges two distinct scenarios characterized by a critical energy $\mathcal{E}_{\rm c} = \delta_c/2$ (i.e., half of the band offset), as indicated by the horizontal pink (dashed) line across the well. In the first scenario, which refers to the

electron energy being below $\mathcal{E}_c$ (i.e., $V_w < \mathcal{E}_c$), the laser field tends to shrink the width of the well. On the other hand, in the second scenario of $V_w > \mathcal{E}_c$, the effective well width appears to be enlarged, cf. dotted and solid curves in Fig. 1(b). The dressing effect induced two scenarios of the variation of the effective well width directly alters the quantum confinement, facilitating flexible control of the Dresselhaus coupling via laser field.

Now we examine the ordering of the critical energy $\mathcal{E}_c$ and the energy levels $\mathcal{E}_1$ and $\mathcal{E}_2$ for the 13-nm well to determine which scenario the two-subband electrons are subject to. For a lower value of the laser parameter with $\alpha_L = 2$ nm, we find that the energy levels of the two subbands are both below $\mathcal{E}_c$, cf. $\mathcal{E}_1$, $\mathcal{E}_2$, and $\mathcal{E}_c$ [Fig. 1(b)]. Thus, both subbands comply with the aforementioned first scenario, in which the quantum confinement for electrons intensifies with the increasing laser parameter due to shrinking of the effective well width. Consequently, as α_L grows, the energy levels of both subbands $\mathcal{E}_1$ and $\mathcal{E}_2$ tend to increase. Thereby, it is rational to conjecture that $\mathcal{E}_2$ will eventually match with $\mathcal{E}_c$ [108], the value of which is pinned at $\delta_c/2$, and further rise above it, resulting in $\mathcal{E}_c$ being sandwiched between $\mathcal{E}_1$ and $\mathcal{E}_2$, as shown in Fig. 1(c) with $\alpha_L = 5$ nm. In other words, for a relatively larger value of the laser parameter, the two subbands may pertain to different scenarios, with the first- and second-subband electrons seeing the effective well width being quenched (first scenario) and widened (second scenario), respectively. The evolution of $\mathcal{E}_1$ and $\mathcal{E}_2$ against α_L reflecting the optical stark effect [62–64] is shown in Fig. 1(d), from which one can find that $\mathcal{E}_2$ and $\mathcal{E}_c$ match at about $\alpha_L = \alpha_{L,c} = 4.8$ nm.

To unveil the laser dressing effect on our self-consistent outcome, we perform a detailed calculation by solving the Schrödinger and Poisson coupled equations for 2D electrons residing in quantum wells within the Hartree approximation. In Fig. 1(e), we show the self-consistent laser dressed potential V_{sc} and wave functions ψ_ν of the two subbands for the 13-nm well with the laser field $\alpha_L = 5$ nm (solid curves). The self-consistent potential in the absence of laser field (i.e., $\alpha_L = 0$) is also shown alongside (dotted curve) for highlighting the laser dressing effect. In addition to the quenching and widening of the effective well width *inherited* from the structural potential V_w, we observe that the laser field also *effectively* lowers the barrier height (i.e., an effective or self-consistent band offset) of the total self-consistent potential V_{sc} seen by electrons, cf. dotted and solid (red) curves in Fig. 1(e). The overall reduction of the self-consistent barrier height, which leads to the weakening of quantum confinement for electrons, is attributed to the laser field modulated electron density and further the resulting electron Hartree potential V_e, see the SM.

The horizontal pink (dashed) line in Fig. 1(e) represents where the critical energy with self-consistence lies, i.e., $\mathcal{E}_c^{sc}$ as indicated by the superscript sc, an analog to $\mathcal{E}_c$ in Figs. 1(b)–1(d) without self-consistence. Even though both the energy levels and the critical energy in their magnitudes are different between the cases of with (e.g., $\mathcal{E}_c^{sc}$) and without (e.g., $\mathcal{E}_c$) self-consistence, the underlying physics about the two scenarios for the change of the effective well width is clearly the same. We should emphasize that the self-consistent $\mathcal{E}_c^{sc}$ varies with the laser field parameter α_L, in contrast to the $\mathcal{E}_c$, which is only related to the structural potential V_w (no self-consistence) and thus maintains a constant of $\delta_c/2$ for all values of α_L.

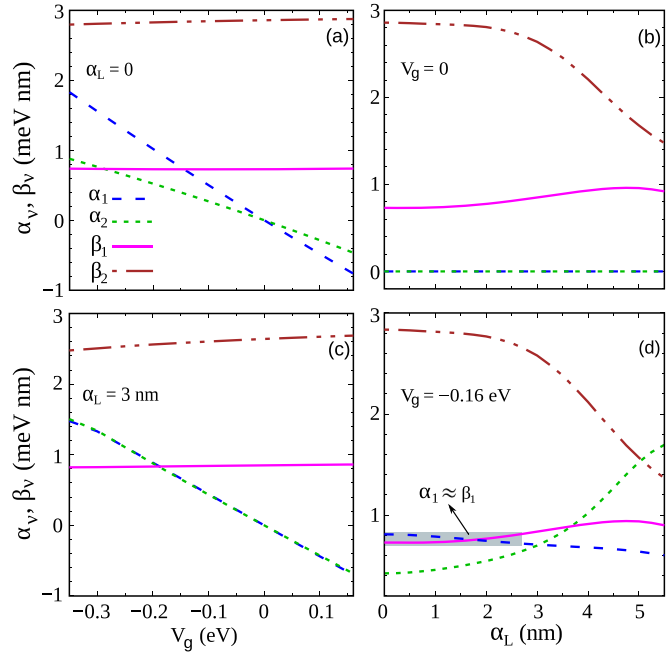

FIG. 2. (a), (b) Rashba α_ν and Dresselhaus β_ν ($\nu = 1, 2$) coefficients as functions of the gate potential V_g at zero laser field (a) and of the laser parameter α_L at zero gate bias (b), for the $Ga_{0.47}In_{0.53}As/Al_{0.48}In_{0.52}As$ well of width $L_w = 13$ nm. (a) and (b) refer to the cases of SO manipulation by purely electrical and optical means, respectively. (c), (d) Dependence of the corresponding SO coefficients on V_g for the well at the laser parameter $\alpha_L = 3$ nm (c) and on α_L at the gate potential $V_g = -0.16$ eV (d). In (d), the shadowed region indicates that the Rashba α_1 and Dresselhaus β_1 coefficients for the first subband essentially match in their magnitudes when α_L ranges from 0 to 2.5 nm.

The above features of our self-consistent dressed potential are helpful in understanding the electro-optical control of SO couplings by gate and laser fields. To unveil the underlying physics systematically, we first examine the SO manipulation by purely electrical and optical means below in Secs. IV B and IV C, respectively.

B. Usual electrical SO control

In Fig. 2(a), we show the gate V_g dependence of the Rashba α_ν and Dresselhaus β_ν coefficients of the two subbands ($\nu = 1, 2$) for the 13-nm well with $\alpha_L = 0$. At zero gate bias, since the well is lack of the SIA, the Rashba coefficients α_1 and α_2 for both subbands identically vanish. When V_g is switched on, the gate bias induced SIA arises, giving rise to nonzero Rashba couplings. As expected, it is found that α_1 and α_2 exhibit similar gate dependence, for which they have the same sign and both increase in magnitude with increasing V_g. Also, the sign of α_1 and α_2 simultaneously reverses when V_g is across zero, as a result of flipping of the gate-induced SIA. Physically, the sign change of α_ν reflects the reversal of the direction of force field [i.e., derivative of potential energy, Eq. (7)] *seen* by electrons, corresponding to flip of SIA [50,81,90]. In general, the Rashba terms of the two subbands

have different strengths, which we mainly attribute to the contribution of the electron Hartree potential V_e [Eq. (7)]. Since the electron Hartree force field (i.e., $F_e = -\partial_z V_e$), in general, has opposite signs on the left and right sides of the well (see the SM), it leads to a compensating effect on contributing to Rashba couplings of the two subbands.

In contrast to the Rashba coupling, the Dresselhaus terms β_1 and β_2, which mainly depend on quantum confinement [e.g., well width], instead of the SIA, are in general barely controlled through electrical means [52], as shown in Fig. 2(a). Below, we resort to the laser field for manipulating the Dresselhaus SO coupling in an optical manner.

As a remark, contrasting values of α_1 and α_2 arise from distinct *local* symmetries seen by electrons of the two subbands. Further, α_1 and α_2 may even possibly have opposite signs [36]. Similarly, the two-subband electrons may also see distinct quantum confinements, giving rise to β_1 and β_2 of the two subbands being different. Note that there is also experimental evidence of the distinction of the Rashba (and Dresselhaus) coefficients between the two subbands, see Refs. [46,109,110].

C. Pure laser-field control of Dresselhaus SO coupling

Figure 2(b) shows the Rashba and Dresselhaus strengths for the 13-nm well with $V_g = 0$, as functions of the laser parameter α_L. Since the laser field maintains the inversion symmetry of the well at zero gate bias [Figs. 1(b) and 1(c)], the Rashba coefficients of the two subbands are zero for all values of α_L. In contrast, for the Dresselhaus coupling, we find that even though β_1 remains essentially constant as the laser field strengthens, β_2 starts to exhibit a considerable reduction when α_L is greater than about 3 nm. The contrasting laser-field dependence of the Dresselhaus terms of the two subbands directly follows from our self-consistent solutions about the two distinct scenarios, which are associated with the ordering of three typical energies of $\mathcal{E}_1$, $\mathcal{E}_2$ and $\mathcal{E}_c^{sc}$ (analog to $\mathcal{E}_c$) (Sec. IV A), as we analyze next.

For electrons occupying the first subband, since the corresponding energy level $\mathcal{E}_1$ constantly lies below the critical energy $\mathcal{E}_c^{sc}$ in the whole range of laser field strengths considered [108], they will see the quantum well with a shrinking width. Meanwhile, the laser dressing effect leads to an overall weakening of quantum confinement of the well because the *effective* (self-consistent) barrier height is reduced. These two compensating contributions to quantum confinement are the resources that lead to β_1 remaining essentially constant as the laser parameter varies.

For the second-subband electrons, the circumstance is in stark contrast. On the one hand, for a lower value of the laser parameter α_L, the relation $\mathcal{E}_2 < \mathcal{E}_c^{sc}$ holds (Sec. IV A). This situation is similar to that for the first subband, resulting in β_2 also being weakly dependent of the laser parameter for α_L less than 3 nm, a value at which $\mathcal{E}_2$ and $\mathcal{E}_c^{sc}$ essentially match. Note that due to the self-consistent correction, here the laser field needed (i.e., $\alpha_L = 3$ nm) to match $\mathcal{E}_2$ and $\mathcal{E}_c^{sc}$ deviates from the one of $\alpha_L = 4.8$ nm, which is based on an illuminating (though lack of self-consistence) estimate for the structural potential V_w only. On the other hand, when α_L is greater than 3 nm, i.e., $\mathcal{E}_2 > \mathcal{E}_c^{sc}$, the electrons occupying the second subband will see the well having not only a widened width but also a lowered offset, both of which weaken the quantum confinement, giving rise to considerable reduction of β_2 with increasing α_L.

D. *Unified* electrical Rashba SO control of distinct subbands mediated by the laser field

Having the knowledge of SO control by purely electrical (Sec. IV B) and optical (Sec. IV C) means, we are ready to turn to the manipulation of SO coupling by both gate and laser fields. We first look into the laser-field mediated electrical control of the Rashba coupling. Figure 2(c) shows the Rashba coefficients of the two subbands as functions of V_g for the 13-nm well with the laser parameter $\alpha_L = 3$ nm. We observe that, in a certain range of laser field strengths, the dressing effect may balance the SIA seen by electrons of the two subbands, resulting in α_1 and α_2 of essentially equal strength at $\alpha_L = 3$ nm. Remarkably, the equality condition of $\alpha_1 = \alpha_2$ remains in the whole range of gate voltages considered here. This continuous locking of α_1 and α_2 to equal strength with varying gate fields provides a means for *unified* manipulation of the two-subband Rashba SO couplings.

For unveiling how the laser field triggers the locking of the Rashba terms of the two subbands, in Fig. 2(d) we show the dependence of SO terms on the laser field for the 13-nm well at $V_g = -0.16$ eV. Note that at zero gate bias both α_1 and α_2 identically vanish due to lack of SIA of the well (symmetric doping condiction), independent of the laser field [Fig. 2(b)]. When the gate potential deviates from zero, we find that α_1 tends to decrease (though very slightly) while α_2 increases as the laser field strengthens. Since α_1 at zero laser field is greater than α_2 because of the distinction of local symmetry seen by electrons of the two subbands, the latter will eventually be equal to the former as α_L increases and further exceeds it. This indicates that even though the laser field does not break the inversion symmetry of a symmetric well at zero bias, it indeed alters the degree of SIA of the well when the gate field is present. The underlying reason is that the dressing effect results in a change of quantum confinement, which alters the energy levels $\mathcal{E}_1$ and $\mathcal{E}_2$ and further the *environment* (symmetry) felt by the first- and second-subband electrons. Here the matching of α_1 and α_2 at $\alpha_L = 3$ nm indicates that when the laser field parameter ranges from 0 to 3 nm, it tends to balance the SIA of the well seen by electrons of the two subbands. We should emphasize that the opposite laser-field control of the two-subband Rashba couplings with more intriguing SO features (e.g., sign change) becomes even more distinct in wider quantum wells, as we will analyze more deeply in Sec. IV F.

E. Matching Rashba and Dresselhaus SO strengths

The Rashba and Dresselhaus SO couplings for electrons act as effective magnetic fields with momentum-dependent directions. This causes spin decay as the spins undergo arbitrary precessions about these randomly oriented SO fields due to momentum scattering [3,80], which usually occurs in 2D diffusive systems. However, when the strengths of Rashba and Dresselhaus terms match, the competing effects of the two

types of SO interactions can (partially) cancel each other out so the total SO field becomes unidirectional, thus rendering the electron spin immune to decay. In this case, a helical spin-density wave excitation, i.e., PSH [17–19,55], emerges for 2D electron gases. Also, for quantum heterostructures with two occupied subbands, we recently revealed that the system can sustain an intriguing spin texture of persistent skyrmion lattice with topological properties [36] when the relevant SO strengths satisfy the condition of $\alpha_1 = \beta_1$ and $\alpha_2 = -\beta_2$ [36], under which the SO fields of the two subbands are crossed.

The matching condition of the Rashba and Dresselhaus SO strengths is usually achieved by resorting to electrical means [34,36,55], as also shown in Fig. 2(d) with $\alpha_1 = \beta_1$ at $V_g = -0.16$ eV. Alternatively, from Fig. 2(d), here we reveal that the state of PSH can also be realized in an optical manner, i.e., via laser field. Remarkably, for the first subband, as both the Rashba and Dresselhaus strengths exhibit weak dependence on α_L, the condition of $\alpha_1 = \beta_1$ essentially remains for a broad range of laser field strengths, see the encircled (shallowed) region in Fig. 2(d). This greatly mitigates the stringency of the matching condition of the Rashba and Dresselhaus SO strengths at a unique value of laser field, highly desirable for practical applications. Further, the essential independence of the $\alpha_1 = \beta_1$ condition (referring to the first subband) on α_L also facilitates the formation of the PSH states for both subbands, as one can just match the Rashba and Dresselhaus strengths of the second subband by fine tuning the laser field.

Note that the locking of matching condition between α_1 and β_1 becomes more distinct for even narrower wells. In the SM, Fig. S2(e) shows the laser field control of Rashba and Dresselhaus SO terms in a 10-nm well, for which the $\alpha_1 = \beta_1$ condition essentially satisfies in an even broader laser field range. Notably, the matching between α_1 and β_1 and between α_2 and β_2 are both achieved at about $\alpha_L = 3.27$ nm, allowing for the simultaneous formation of persistent spin helices for the two subbands. Also, here we mainly focus on the general picture of the laser field controlled PSH, for which the linear Dresselhaus term, in general, dominates over the cubic one, with the latter breaking the SU(2) symmetry of the PSH state and leading to spin decay. Strictly speaking, one also needs to take into account the detrimental cubic term to determine a more precise condition that the PSH forms by introducing a renormalized linear Dresselhaus term as we did in recent works [34,36,81].

We should emphasize that the two ways, i.e., the electrical (gate field) and optical (laser field) means, are complementary to each other in facilitating control of various SO terms. For purely electrical means, since the linear Dresselhaus terms β_ν mainly depend on quantum confinement (rather than the symmetry of the system) and is essentially immune to electrical control, this to a certain extent restrains the flexibility of controlling the PSH [34]. The advantage of the laser field is that it is feasible to achieve flexible control of the linear Dresselhaus term, in particular, for the second subband, in addition to the Rashba and cubic Dresselhaus terms. On the other hand, when the gate bias is zero, the system is in the symmetric configuration, under which no matter what the light intensity and laser frequency are, the Rashba term maintains zero. Remarkably, by combing the two ways, it even eases the difficulty of simultaneously achieving the PSH states

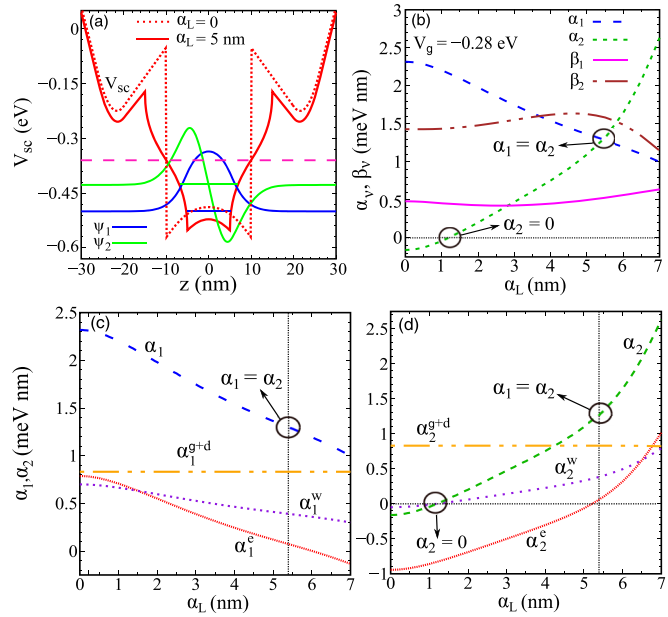

FIG. 3. (a) Zero-bias self-consistent potential V_{sc} and wave functions ψ_ν for the 20-nm well at $\alpha_L = 5$ nm, with the dotted (red) curve referring to V_{sc} at $\alpha_L = 0$. The horizontal blue (green) line inside the well indicates the energy level $\mathcal{E}_1$ ($\mathcal{E}_2$) of the first (second) subband, and the horizontal pink (dashed) line across the well refers to the critical energy $\mathcal{E}_c^{sc}$ with self-consistence. (b) Rashba α_ν and Dresselhaus β_ν SO coefficients versus α_L for the well at $V_g = -0.28$ eV. The left (right) black circle indicates $\alpha_2 = 0$ ($\alpha_1 = \alpha_2$) occurring at $\alpha_L = 1.19$ nm (5.42 nm). (c), (d) Distinct contributions to the Rashba strength of the first (c) and second (d) subbands as functions of α_L, including the gate plus doping contribution α_ν^{g+d}, the electron Hartree contribution α_ν^{e}, and the structural contribution (with the laser dressing effect) α_ν^{w}.

of the two subbands. The key is that one can just tune α_2 and β_2 to equal strength since α_1 and β_1 turn to essentially remain locked to equal strength as the laser field varies [cf. Figs. 2(d) and S2(e)], providing an ideal platform for exploring two copies of PSHs in quantum systems.

F. Electro-optical SO control for a relatively wide well

Now, we move to another regime of electro-optical control of the SO terms in a relatively wide well of $L_w = 20$ nm. In Fig. 3(a), we show the self-consistent potential and wave functions of the two subbands for the 20-nm well at zero gate bias. It is found that the general feature of the laser dressing effect on the potential profile is similar to that for the 13-nm well, cf. dotted and solid (red) curves for the potential profile with the laser parameter $\alpha_L = 0$ and 5 nm, respectively. However, due to weak quantum confinement in a wide well, here the energy levels $\mathcal{E}_1$ and $\mathcal{E}_2$ of the two subbands are both below the critical value of $\mathcal{E}_c^{sc}$, which characterizes two distinct scenarios for the change of the effective well width due to the laser dressing effect, even at a higher laser field strength of $\alpha_L = 5$ nm, cf. the horizontal blue (green) lines inside the well for $\mathcal{E}_1$ ($\mathcal{E}_2$) and the pink (dashed) line across the well for $\mathcal{E}_c^{sc}$. This indicates that the two subbands both comply with the first scenario (Sec. IV A) in the whole range

of laser field strengths considered, in contrast to that for the 13-nm well.

Figure 3(b) shows the Rashba and Dresselhaus SO coefficients as functions of the laser parameter for the 20-nm well at $V_g = -0.28$ eV. We first look into the laser field dependence of Dresselhaus terms. Since both subbands comply with the first scenario, in which the energy levels $\mathcal{E}_1$ and $\mathcal{E}_2$ and the critical energy $\mathcal{E}_c^{sc}$ are in ascending order, the compensating effect of the effective well width and the self-consistent band offset on quantum confinement (Sec. IV A), results in β_1 and β_2 remaining weakly dependent of the laser field for all values of α_L considered. This is in contrast to that of the 13-nm well for which $\mathcal{E}_2$ could be either below or above $\mathcal{E}_c^{sc}$, depending on the strength of laser field, cf. Figs. 3(b) and 2(d). On the other hand, for the Rashba coupling, as the laser parameter varies, we reveal that the Rashba coefficients α_1 and α_2 of the two subbands could have either the same or opposite signs, or even α_2 vanishes while α_1 is finite, greatly fascinating for selective SO manipulation. Below we analyze these features in more detail.

We reveal two contrasting regimes for the laser field control of the Rashba coupling, marked off by the laser parameter at $\alpha_L = \alpha_{L,\mathcal{R}} \sim 1.19$ nm, as indicated by the left (black) circle in Fig. 3(b). Specifically, for α_L being greater and lower than $\alpha_{L,\mathcal{R}}$, we find that the Rashba coefficients α_1 and α_2 have the same and opposite signs, respectively. This makes it feasible for tuning the persistent spin helices of the two subbands [17–19] being collinear or "crossed" through the laser field, with the latter crossed case even resembling the topologically nontrivial skyrmion-lattice spin density excitation, i.e., persistent skyrmion lattice [36]. Further, in the first regime of $\alpha_L < \alpha_{L,\mathcal{R}}$, the amplitudes of α_1 and α_2, which have opposite signs, reduce as the laser field strengthens, while in the second regime for $\alpha_L > \alpha_{L,\mathcal{R}}$, they have the same sign and exhibit opposite dependence on α_L, greatly fascinating for selective control of the SO couplings of distinct subbands.

Right at the point of $\alpha_L = \alpha_{L,\mathcal{R}}$ bridging the two regimes, it is clear that α_2 identically vanishes while α_1 is finite, see the left (black) circle in Fig. 3(b). We first proposed in Ref. [81] that the condition of $\alpha_1 \neq 0$ and $\alpha_2 = 0$ could simultaneously hold. Here we achieve this condition by fine-tuning the laser field. To better understand this, in Fig. 4(a) we show the self-consistent outcome for the well at $\alpha_L = \alpha_{L,\mathcal{R}}$. It is found that ψ_1 and ψ_2 of the two subbands tend to localize on opposite sides of the well. Specifically, the electrons of the first-subband are apt to be localized on the right side of the well, while the second-subband electrons tend to be concentrated on the left side, cf. ψ_1 and ψ_2 in Fig. 4(a). This enables the feasibility of vanishing α_2 even for an asymmetric quantum well, due to the delicate cancellation of contributions from the electron Hartree potential and the gate plus doping potential to the Rashba coupling [Eq. (7)]. And, within the second regime of $\alpha_L > \alpha_{L,\mathcal{R}}$, as a result of contrasting dependence of α_1 and α_2 on the laser field, we reveal that they match with not only the same sign but also the same magnitude at about $\alpha_L = 5.42$ nm. Further, it is remarkable that when α_L is around 5.42 nm, due to a *delicate* interplay of the laser and gate fields, we find that even though the quantum well at $V_g = -0.28$ eV is structurally asymmetric, it attains a *seemingly* symmetric configuration, as shown in Fig. 4(b) for

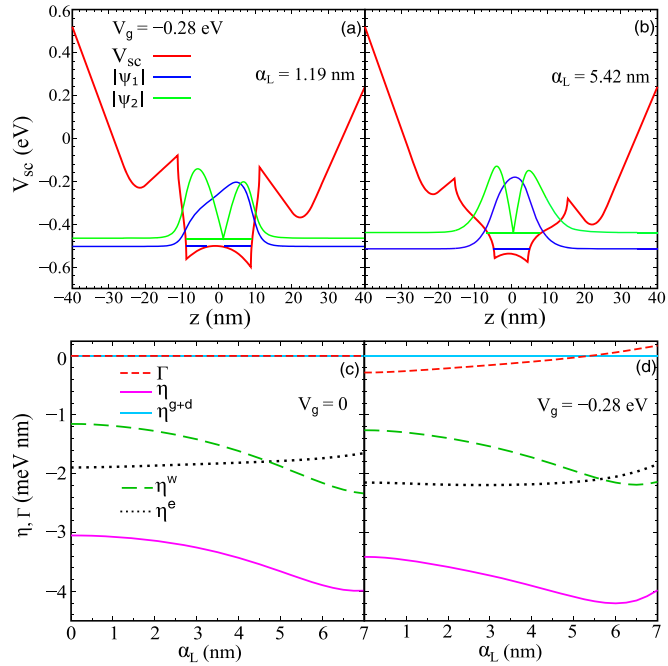

FIG. 4. Self-consistent potential V_{sc} and wave functions ψ_ν ($\nu = 1, 2$) for the 20-nm well at $\alpha_L = 1.19$ (a) and 5.42 nm (b). The horizontal blue (green) line inside the well indicates the energy level $\mathcal{E}_1$ ($\mathcal{E}_2$) of the first (second) subband. (c), (d) Dependence of the intersubband Rashba η and Dresselhaus Γ coefficients on α_L for the well at $V_g = 0$ (c) and -0.28 eV (d). In (a) and (b), the gate potential is chosen as $V_g = -0.28$ eV; in (c) and (d), several contributions to η are also shown, including the gate plus doping η^{g+d}, the electron Hartree η^e and the laser dressed structural η^w contributions.

the self-consistent solutions. From Fig. 4(b), we can see that the electrons occupying the two subbands are almost equally distributed on the left and right sides of the well, despite the potential in its profile embracing an overall inversion asymmetry. This indicates that, as the laser field increases, it may to a certain extent balance the electron distributions between the left and right sides of the well, cf. Figs. 4(a) and 4(b).

To further explore the underlying physics beneath the electro-optical control of the Rashba coupling, in Figs. 3(c) and 3(d), we show the Rashba coefficients of the two subbands and the corresponding constituent contributions as functions of α_L for the 20-nm well at $V_g = -0.28$ eV. For the gate plus doping contribution α_ν^{g+d}, since the corresponding potential V_{g+d} is linear across the well region (see the SM), which refers to a constant force field of $F_{g+d} = -dV_{g+d}/dz$, it is straightforward that the equality $\alpha_1^{g+d} = \alpha_2^{g+d}$ follows. In contrast to α_ν^{g+d}, the electron Hartree contributions α_1^e and α_2^e essentially have opposite signs, cf. α_1^e [Fig. 3(c)] and α_2^e [Fig. 3(d)]. This is because the electrons occupying the first and second subbands tend to reside in different sides of the well. As a result, the electron Hartree force field $F_e = -dV_e/dz$ felt by the two-subband electrons are mostly opposite in the sign across the well region. Clearly, it is the electron Hartree contribution α_ν^e dominating why the total Rashba coefficients α_1 and α_2 may have opposite signs. Further, both α_1^e and α_2^e basically vanish around α_L equal to 5.42 nm, following from that the system

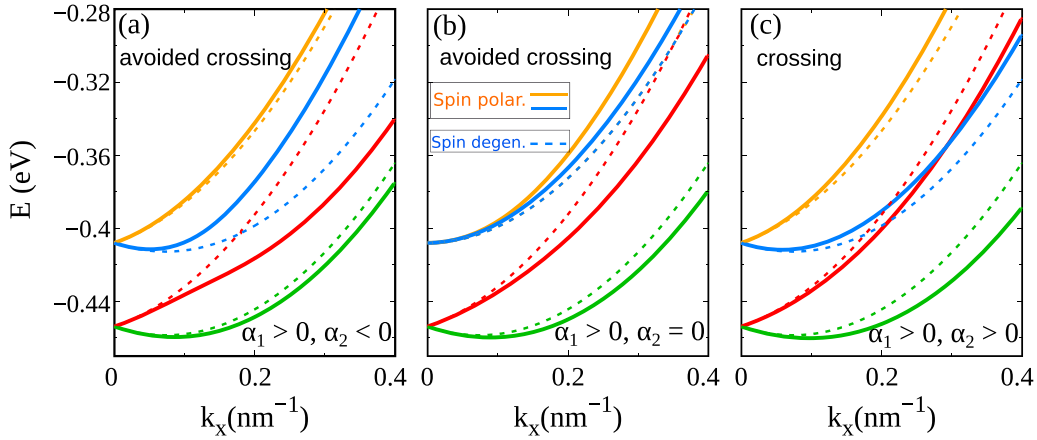

FIG. 5. Rashba band dispersion (scaled by a factor of 100 for visibility) with both intra- and intersubband SO terms versus k_x [|| (100)] of the AlInAs/GaInAs well, for $\{\alpha_1 > 0, \alpha_2 < 0\}$ (a), $\{\alpha_1 > 0, \alpha_2 = 0\}$ (b), and $\{\alpha_1 > 0, \alpha_2 > 0\}$ (c). The dotted curves correspond to the uncoupled ($\eta = 0$) bands, and for $\eta \neq 0$ the bands exhibit avoided crossing (a), (b), or maintain crossing (c), depending on the combined effect of intra- and intersubband terms. (a)–(c) refer to three distinct scenarios, which can be tunable via varying the laser field. The magnitudes of Rashba coefficients are chosen for the 20-nm well at $V_g = -0.28$ eV and $\alpha_L = 5.42$ nm [Figs. 3(b) and 4(d)], i.e., $\alpha_1 = -\alpha_2 = 1.3$ meV nm for (a), $\alpha_1 = 1.3$ meV nm, $\alpha_2 = 0$ for (b), and $\alpha_1 = \alpha_2 = 1.3$ meV nm for (c), and $\eta = -4.15$ meV nm. In (b), the combined effect of intra- and intersubband SO terms triggers the spin polarization for the second subband from an initially spin degenerate (unpolarized) one.

features a *seemingly* symmetric configuration [Fig. 4(b)], as expected. Regarding the constituent contribution from the laser dressed structural potential, i.e., α_1^w and α_2^w, we find that the former decreases while the latter increases as the laser field strengthens, arising from the laser field modulated electron redistributions between the left and right sides of the well.

Now we further analyze how α_2 can be zero for a well with the SIA in terms of its constituent contributions. According to Ehrenfest's theorem, there's always $\langle\partial_z V\rangle_\nu = \langle\psi_\nu|\partial_z(V_w + V_g + V_d + V_e)|\psi_\nu\rangle = 0$, namely, $\langle\psi_\nu|\partial_z V_w|\psi_\nu\rangle = -\langle\psi_\nu|\partial_z(V_g + V_d + V_e)|\psi_\nu\rangle$, from which the Rashba term given in Eq. (7) rereads $\alpha_\nu = (1 - \eta_H/\eta_w)\alpha_\nu^w$. That means that α_ν is equal to α_ν^w up to a constant prefactor, implying that when the structural contribution is zero the total Rashba coefficient is bound to vanish, cf. α_2^w and α_2 in Fig. 3(d). The vanishing Rashba coupling for a given subband can in principle be used to selectively suppress the SO-induced spin relaxation mechanisms among distinct subbands.

G. Intersubband Rashba and Dresselhaus couplings

Figures 4(c) and 4(d) show the intersubband Rashba coupling η including its constituent contributions $\eta^{g+d,e,w}$ and the Dresselhaus coupling Γ for the 20-nm well at $V_g = 0$ (-0.28 eV). At zero gate bias, the well is structurally symmetric. Thus, due to distinct parities of the wave functions ψ_1 and ψ_2 of the two subbands, the Dresselhaus strength Γ, independent of the strength of laser field, maintains zero [Fig. 4(c)]. On the other hand, when the gate bias is switched on with $V_g = -0.28$ eV, even though Γ is mostly finite as the laser parameter varies, we observe that it vanishes again at about $\alpha_L = 5.42$ nm [Fig. 4(d)], for which the well embraces a *seemingly* symmetric configuration [Fig. 4(b)]. And, as the laser parameter further increases, the sign of Γ is even reversed, similar to the gate dependence of intrasubband Rashba terms [Fig. 2(a)].

Regarding the Rashba strength $|\eta| = |\eta^{g+d} + \eta^e + \eta^w|$, it mainly depends on the overlap of the wave functions of the two subbands. As a result, η is even approaching its maximal value at about $\alpha_L = 5.42$ nm, for which the distributions of the two-subband wave functions are essentially symmetric. This is in stark contrast to the intersubband term Γ, which identically vanishes in symmetric configuration due to distinct parities of ψ_1 and ψ_2. And, because of the orthogonality condition of ψ_1 and ψ_2, the gate plus doping contribution η^{g+d} remains zero in either case of the gate bias being switched on or off [Figs. 4(c) and 4(d)], following from the gate plus doping potential V_{g+d} being linear (i.e., $\partial_z V_{g+d}$ is constant) across the well region (see the SM). Therefore, the intersubband Rashba term essentially only depends on the electron Hartree η^e and the structural η^w contributions. Despite detailed SO features, we should emphasize that the intersubband terms are, in general, weakly dependent of the gate or laser fields.

For a complete picture of the gate dependence of intersubband SO couplings, in the SM we show the full electric swing ($\alpha_L = 0$) of Γ and η within both positive and negative V_g ranges (Fig. S3). When V_g varies from positive to negative values, we reveal that the sign of Γ will be switched, similar to intrasubband Rashba coefficients α_ν [see Figs. 2(a) and 2(c)]. This is in contrast to intrasubband Dresselhaus coefficients β_ν, which mainly depend on quantum confinement and are essentially immune to electrical control [see Figs. 2(b) and 2(d)]. Referring to η, which mainly depends on the overlap of wave functions of the two subbands, it together with its constituent contributions (i.e., η^j, j = g + d, w, e) remains the same sign in the whole range of gate fields considered.

H. Combined effect of intra- and intersubband SO terms

By adjusting the laser field, as we have already revealed, the Rashba coefficients α_1 and α_2 of the two subbands may have the same or opposite signs, or even when α_2 vanishes while α_1 is finite [Figs. 3(b)–3(d)]. This together with the

intersubband SO term may lead to intriguing SO effects. For simplicity, here we mainly focus on the Rashba band dispersion. A neat form of the 4×4 matrix form of the two-subband Rashba model with analytical solutions is given in the SM. In Figs. 5(a)–5(c), we show the Rashba dispersions with both intra- and intersubband SO terms, in the cases of $\{\alpha_1 > 0, \alpha_2 < 0\}$, $\{\alpha_1 > 0, \alpha_2 = 0\}$ and $\{\alpha_1 > 0, \alpha_2 > 0\}$, respectively. It is found that the combined effect of intra- and intersubband SO couplings may lead to avoided crossings among distinct spin branches of the two subbands, when α_1 and α_2 have opposite signs [Fig. 5(a)] or even when α_2 vanishes while α_1 is finite [Fig. 5(b)]. In contrast, when α_1 and α_2 have same sign, the crossing feature remains as compared to the uncoupled (i.e., $\eta = 0$) bands [Fig. 5(c)]. Notably, in the case of $\alpha_2 = 0$ [Fig. 5(b)], the second subband which is initially spin unpolarized [dotted (blue) curves for spin-degenerate branches], may become spin polarized [solid (yellow and blue) curves for spin-split branches], entirely because of the interplay of intra- and intersubband SO interactions. Specifically, the intersubband term behaves as a *media* between the two subbands and *transfers* the spin polarization of the first subband to the second one.

The intersubband SO interaction induced avoided crossings have been experimentally verified in Rashba surface states of Bi/Ag(111) and Bi/Cu(111) [46,111] even with hybridized spin textures. Very recently, Song *et al.* put forward an unconventional two-band Rashba model with distinct symmetries between intra- and intersubband terms, giving rise to giant inverse Rashba-Edelstein Effect [112]. In addition, the intersubband term also underpins several other spin-related phenomena including the intrinsic spin Hall effect [47,113], spin filtering [114], and unusual *zitterbewegung* [115,116]. Also, when the Rashba and Dresselhaus SO terms (both intra- and intersubband terms) coexist, the underlying physics about hybridized spin textures and the resulting novel SO features may even be enriched. As future works, it would be interesting to explore these various intriguing possibilities.

V. CONCLUDING REMARKS

The Dresselhaus SO coupling mainly depends on quantum confinement (e.g., well width), thus it is, in general, hardly controlled by electrical means, in contrast to the Rashba term, which is associated with the SIA of the system. Here we have theoretically reported the optical manipulation of SO couplings by resorting to IHFL, which features the so-called dressing effect and greatly alters the confining potential for electrons. This enables a flexible and simultaneous control of the Rashba and Dresselhaus couplings, highly desirable for practical considerations. Focusing on ordinary GaInAs/AlInAs quantum wells with two occupied subbands subject to both laser and gate fields, we have performed a self-consistent Poisson-Schrödinger calculation within the Hartree approximation to determine electro-optical control of the intrasubband (intersubband) Rashba α_ν (η) and Dresselhaus β_ν (Γ) SO terms with $\nu = 1, 2$.

With the mediation of laser field, we have achieved *continuous* locking of the Rashba terms α_1 and α_2 of the two subbands to equal strength in a broad gate range, providing a means for *unified* manipulation of the two-subband Rashba couplings. Further, as the laser field varies, we observe that α_1 and α_2 may have either the same or opposite signs, or even α_2 vanishes while α_1 is finite, greatly fascinating for selective SO control of distinct subbands. For the Dresselhaus coupling, we disclose two distinct scenarios depending on the interplay of the well width and the laser field strength and reveal that β_2 may decrease rapidly when the laser field strengthens, even though β_1 remains essentially constant. Regarding the intersubband Rashba (η) and Dresselhaus (Γ) terms, which mainly depend on the overlap and parity of the wave functions of the two subbands, they have relatively weak dependence on the laser field. Moreover, the interplay of intra- and intersubband SO terms may lead to crossings and avoided crossings of the energy dispersion of multiband spin branches and may even trigger the spin poarlization of an originally spin degenerate (unpolarized) band, tunable by the laser field. Our results should stimulate experiments probing the laser field mediated multiband SO control and further enables its spintronic applications.

Further, we are restricted to either the high-frequency regime of $\omega\tau \gg 1$ or the high-intensity regime of $I \sim I_c = m^{*2}\alpha_B^{*2}\omega^4 c\epsilon_0\epsilon_r^{1/2}/2e^2$ (see Sec. III). On the one hand, the laser-field range with frequency of hundreds of THz and intensity of about 10^{12} W/cm^2 that we consider are widely adopted in experiments [58,102–105], ensuring our results are feasible for future experimental realizations. On the other hand, while here we focus on a nonresonant laser field, i.e., without both intersubband (conduction-conduction bands) and interband (conduction-valence bands) transitions [97], the SO-mediated linear (and nonlinear) spin-dependent optical properties as well as the spin dynamics and transport in the near-resonance scenario with phonon relaxation (depending on the detuning of laser field frequency with intersubband energy separation) and even impurity scattering may be interesting. More work is needed to explore these possibilities.

As a final remark, we recently explored in detail the Rashba and Dresselhaus SO interactions for wide-gap semiconductor heterostructures in the wurtzite phase (e.g., GaN/AlNGa) in Ref. [117]. Due to strong built-in fields (spontaneous and piezoelectric) in such quantum systems, it is even unreasonable to achieve through electrical means a flexible control of the Rashba term, let alone the Dresselhaus coupling. By resorting to the IHFL field that we proposed here, it may even enable full control of the two types of SO couplings in heterostructures with strong built-in electrical fields .

ACKNOWLEDGMENTS

This work was supported by the National Natural Science Foundation of China (Grants No. 12274256, No. 11874236, No. 12022413, No. 11674331, and No. 61674096), the Major Basic Program of Natural Science Foundation of Shandong Province (Grant No. ZR2021ZD01), the "Strategic Priority Research Program (B)" of the Chinese Academy of Sciences (Grant No. XDB33030100) and the Brazilian funding agencies CNPq, CAPES, and FAPDF. S.X.H. was partially supported by Shandong Provincial Natural Science Foundation (Grant No. ZR2019BA007). W.L. acknowledges financial support from the Higher Educational Youth Innovation Science and Technology Program of Shandong Province (Grant No. 2019KJJ010)

[1] D. Awschalom, D. Loss, and N. Samarth, *Semiconductor Spintronics and Quantum Computation* (Springer, New York, 2002)

[2] I. Žutić, J. Fabian, and S. D. Sarma, Spintronics: Fundamentals and applications, Rev. Mod. Phys. **76**, 323 (2004).

[3] J. Fabian, A. Matos-Abiague, C. Ertler, P. Stano, and I. Žutić, Semiconductor Spintronics, Acta Phys. Slovaca **57**, 565 (2007).

[4] J. Sklenar, W. Zhang, M. B. Jungfleisch, W. J. Jiang, H. Saglam, J. E. Pearson, J. B. Ketterson, and A. Hoffmann, Perspective: Interface generation of spin-orbit torques, J. Appl. Phys. **120**, 180901 (2016).

[5] Y. C. Lau, D. Betto, K. Rode, J. M. D. Coey, and P. Stamenov, Spin-orbit torque switching without an external field using interlayer exchange coupling, Nat. Nanotechnol. **11**, 758 (2016).

[6] S. D. Ganichev, E. L. Ivchenko, V. V. Bel'kov, S. A. STarasenko, M. Sollinger, D. Weiss, W. Wegscheider, and W. Prettl, Spin-galvanic effect, Nature **417**, 153 (2002).

[7] B. A. Bernevig, T. L. Hughes, and S. C. Zhang, Quantum spin Hall effect and topological phase transition in HgTe quantum wells, Science **314**, 1757 (2006).

[8] R. M. Lutchyn, J. D. Sau, and S. Das Sarma, Majorana Fermions and a Topological Phase Transition in Semiconductor-Superconductor Heterostructures, Phys. Rev. Lett. **105**, 077001 (2010).

[9] G. Oreg, Y. Refael, and F. von Oppen, Helical Liquids and Majorana Bound States in Quantum Wires, Phys. Rev. Lett. **105**, 177002 (2010).

[10] R. Song, P. Zhang, and N. Hao, Phase-Manipulation-Induced Majorana Mode and Braiding Realization in Iron-Based Superconductor Fe(Te,Se), Phys. Rev. Lett. **128**, 016402 (2022).

[11] H. M. Weng, C. Fang, Z. Fang, B. A. Bernevig, and X. Dai, Weyl Semimetal Phase in Noncentrosymmetric Transition-Metal Monophosphides, Phys. Rev. X **5**, 011029 (2015).

[12] Y. A. Bychkov and E. I. Rashba, Properties of a 2D electron gas with lifted spectral degeneracy, JETP Lett. **39**, 78 (1984).

[13] G. Dresselhaus, Spin-orbit coupling effects in zinc blende structures, Phys. Rev. **100**, 580 (1955).

[14] M. D'yakonov, V. Marushchak, V. Perel', and A. Titkov, The effect of strain on the spin relaxation of conduction electrons in III-V semiconductors, Sov. Phys. JETP **63**, 655 (1986).

[15] Y. Yafet, Conduction electron spin relaxation in the superconducting state, Phys. Lett. A **98**, 287 (1983).

[16] J. Schliemann, J. C. Egues, and D. Loss, Nonballistic Spin-Field-Effect Transistor, Phys. Rev. Lett. **90**, 146801 (2003).

[17] B. A. Bernevig, J. Orenstein, and S.-C. Zhang, Exact SU(2) Symmetry And Persistent Spin Helix in a Spin-Orbit Coupled System, Phys. Rev. Lett. **97**, 236601 (2006).

[18] J. D. Koralek, C. P. Weber, J. Orenstein, B. A. Bernevig, S.-C. Zhang, S. Mack, and D. D. Awschalom, Emergence of the persistent spin helix in semiconductor quantum wells, Nature **458**, 610 (2009).

[19] M. P. Walser, C. Reichl, W. Wegscheider, and G. Salis, Direct mapping of the formation of a persistent spin helix, Nat. Phys. **8**, 757 (2012).

[20] PSH patterns for 2DEGs in the ballistic regime were studied by M. H. Liu, K. W. Chen, S. H. Chen, and C.-R. Chang, Phys. Rev. B **74**, 235322 (2006); see, also, M. H. Liu, C.-R. Chang, and S . H. Chen, *ibid.* **71**, 153305 (2005); for other ballistic spin textures. In addition, a symmetry-based discussion of PSHs in hole gases can be found in Dollinger, M. Kammermeier, A. Scholz, P. Wenk, J. Schliemann, K. Richter, and R. Winkler, *ibid.* **90**, 115306 (2014).

[21] P. Altmann, F. G. G. Hernandez, G. J. Ferreira, M. Kohda, C. Reichl, W. Wegscheider, and G. Salis, Current Controlled Spin Precession of Quasistationary Electrons in a Cubic Spin-Orbit Field, Phys. Rev. Lett. **116**, 196802 (2016).

[22] Y. Kunihashi, H. Sanada, H. Gotoh, K. Onomitsu, M. Kohda, J. Nitta, and T. Sogawa, Drift transport of helical spin coherence with tailored spin–orbit interactions, Nat. Commun. **7**, 10722 (2016).

[23] S. Anghel, A. V. Poshakinskiy, K. Schiller, F. Passmann, C. Ruppert, S. A. Tarasenko, G. Yusa, T. Mano, T. Noda, and M. Betz, Anisotropic Expansion of Drifting Spin Helices in GaAs Quantum Wells, Phys. Rev. B **103**, 035429 (2021).

[24] F. G. G. Hernandez, G. J. Ferreira, M. Luengo-Kovac, V. Sih, N. M. Kawahala, G. M. Gusev, and A. K. Bakarov, Electrical control of spin relaxation anisotropy during drift transport in a two-dimensional electron gas, Phys. Rev. B **102**, 125305 (2020).

[25] D. Iizasa, A. Aoki, T. Saito, J. Nitta, G. Salis, and M. Kohda, Control of spin relaxation anisotropy by spin-orbit-coupled diffusive spin motion, Phys. Rev. B **103**, 024427 (2021).

[26] J. Ishihara, Y. Ohno, and H. Ohno, Direct imaging of gate-controlled persistent spin helix state in a modulation-doped GaAs/AlGaAs quantum well, Appl. Phys. Express **7**, 013001 (2014).

[27] Y. Y. Tkach, Identification of a state of persistent spin helix in a parallel magnetic field, and exploration of its transport properties, Phys. Rev. B **105**, 165409 (2022).

[28] H. Liu, W. E. Liu, S. Chesi, R. Joynt, and D. Culcer, Phase diagram of the interacting persistent spin-helix state, Phys. Rev. B **102**, 205410 (2020).

[29] M. Kammermeier, P. Wenk, and J. Schliemann, Control of spin Helix Symmetry in Semiconductor Quantum Wells by Crystal Orientation, Phys. Rev. Lett. **117**, 236801 (2016).

[30] M. Kammermeier, A. Seith, P. Wenk, and J. Schliemann, Persistent spin textures and currents in wurtzite nanowire-based quantum structures, Phys. Rev. B **101**, 195418 (2020).

[31] K. Yoshizumi, A. Sasaki, M. Kohda, and J. Nitta, Gate-controlled switching between persistent and inverse persistent spin helix states, Appl. Phys. Lett. **108**, 132402 (2016).

[32] M. Alidoust, Critical supercurrent and φ_0 state for probing a persistent spin helix, Phys. Rev. B **101**, 155123 (2020).

[33] M. Alidoust, C. H. Shen, and I. Žutić, Cubic spin-orbit coupling and anomalous Josephson effect in planar junctions, Phys. Rev. B **103**, L060503 (2021).

[34] F. Dettwiler, J. Y. Fu, S. Mack, P. J. Weigele, J. C. Egues, D. D. Awschalom, and D. M. Zumbühl, Stretchable Persistent Spin Helices in GaAs Quantum Wells, Phys. Rev. X **7**, 031010 (2017).

[35] P. J. Weigele, D. C. Marinescu, F. Dettwiler, J. Fu, S. Mack, J. C. Egues, D. D. Awschalom, and D. M. Zumbuhl, Symmetry breaking of the persistent spin helix in quantum transport, Phys. Rev. B **101**, 035414 (2020).

[36] J. Y. Fu, P. H. Penteado, M. O. Hachiya, D. Loss, and J. C. Egues, Persistent Skyrmion Lattice of Noninteracting Electrons with Spin-Orbit Coupling, Phys. Rev. Lett. **117**, 226401 (2016).

[37] J. Schliemann, Colloquium: Persistent spin textures in semiconductor nanostructures, Rev. Mod. Phys. **89**, 011001 (2017).

[38] M. Kohda and G. Salis, Physics and application of persistent spin helix state in semiconductor heterostructures, Semicond. Sci. Technol. **32**, 073002 (2017).

[39] G. Engels, J. Lange, T. Schäpers, and H. Lüth, Experimental and theoretical approach to spin splitting in modulation-doped $In_xGa_{(1-x)}As/InP$ quantum wells for $B \to 0$, Phys. Rev. B **55**, R1958 (1997).

[40] J. Nitta, T. Akazaki, H. Takayanagi, and T. Enoki, Gate Control of Spin-Orbit Interaction in an Inverted $In_{0.53}Ga_{0.47}As/In_{0.52}Al_{0.48}As$, Phys. Rev. Lett. **78**, 1335 (1997).

[41] N. S. Averkiev, L. E. Golub, and M. Willander, Spin relaxation anisotropy in two-dimensional semiconductor systems, J. Phys.: Condens. Matter **14**, R271 (2002).

[42] N. S. Averkiev and L. E. Golub, Giant spin relaxation anisotropy in zinc-blende heterostructures, Phys. Rev. B **60**, 15582 (1999).

[43] C.-M. Hu, J. Nitta, T. Akazaki, H. Takayanagai, J. Osaka, P. Pfeffer, and W. Zawadzki, Zero-field spin splitting in an inverted $In_{0.53}Ga_{0.47}As/In_{0.52}Al_{0.48}As$ heterostructure: Band nonparabolicity influence and the subband dependence, Phys. Rev. B **60**, 7736 (1999).

[44] Q. X. Wang, H. Yang, and J. Y. Fu, Selective asymmetric gate control of the Rashba spin-orbit coupling in GaInAs/AlInAs stepped wells, Phys. Rev. B **101**, 245403 (2020).

[45] C.-M. Hu, J. Nitta, T. Akazaki, H. Takayanagi, J. Osaka, P. Pfeffer, and W. Zawadzki, Observation of the zero-field spin splitting of the second subband in an inverted $In_{0.53}Ga_{0.47}As/In_{0.52}Al_{0.48}As$ heterostructure, Physica E **6**, 767 (2000).

[46] H. Bentmann, S. Abdelouahed, M. Mulazzi, J. Henk, and F. Reinert, Direct Observation of Interband Spin-Orbit Coupling in a Two-Dimensional Electron System, Phys. Rev. Lett. **108**, 196801 (2012).

[47] F. G. G. Hernandez, L. M. Nunes, G. M. Gusev, and A. K. Bakarov, Observation of the intrinsic spin Hall effect in a two-dimensional electron gas, Phys. Rev. B **88**, 161305(R) (2013).

[48] E. A. de Andrada e Silva, G. C. La Rocca, and F. Bassani, Spin-orbit splitting of electronic states in semiconductor asymmetric quantum wells, Phys. Rev. B **55**, 16293 (1997).

[49] R. S. Calsaverini, E. Bernardes, J. C. Egues, and D. Loss, Intersubband-induced spin-orbit interaction in quantum wells, Phys. Rev. B **78**, 155313 (2008).

[50] W. Liu, H. Yang, and J. Y. Fu, Unusual spin-orbit control in AlInAs/GaInAs triple wells triggered by band crossing and anticrossing, Phys. Rev. B **104**, 165428 (2021).

[51] M. P. Walser, U. Siegenthaler, V. Lechner, D. Schuh, S. D. Ganichev, W. Wegscheider, and G. Salis, Dependence of the Dresselhaus spin-orbit interaction on the quantum well width, Phys. Rev. B **86**, 195309 (2012).

[52] Our recent findings show that the band crossing and anticrossing in multiband and multiwells may facilitate electrical control of the Dresselhaus SO coupling.

[53] G. J. Ferreira, F. G. G. Hernandez, P. Altmann, and G. Salis, Spin drift and diffusion in one-and two-subband helical systems, Phys. Rev. B **95**, 125119 (2017).

[54] I. R. de Assis, R. Raimondi, and G. J. Ferreira, Spin drift-diffusion for two-subband quantum wells, Phys. Rev. B **103**, 165304 (2021).

[55] A. Sasaki, S. Nonaka, Y. Kunihashi, M. Kohda, T. Bauernfeind, T. Dollinger, K. Richter, and J. Nitta, Direct determination of spin-orbit interaction coefficients and realization of the persistent spin helix symmetry, Nat. Nanotechnol. **9**, 703 (2014).

[56] W. C. Henneberger, Perturbation Method for Atoms in Intense Light Beams, Phys. Rev. Lett. **21**, 838 (1968).

[57] Q. Fanyao, A. L. A. Fonseca, and O. A. C. Nunes, Hydrogenic impurities in a quantum well wire in intense, high-frequency laser fields, Phys. Rev. B **54**, 16405 (1996).

[58] M. E. Corrales, J. González-Vazquez, G. Balerdi, I. R. ISolá, R. de Nalda, and L. Banares, Control of ultrafast molecular photodissociation by laser-field-induced potentials, Nat. Chem. **6**, 785 (2014).

[59] H. Lakhotia, H. Y. Kim, M. Zhan, S. Hu, S. Meng, and E. Goulielmakis, Laser picoscopy of valence electrons in solids, Nature **583**, 55 (2020).

[60] A. S. Durmuslar, M. E. Mora-Ramos, and F. Ungan, Nonlinear optical properties of n-type asymmetric double δ-doped quantum wells: role of high-frequency laser radiation, doping concentration and well width, Eur. Phys. J. Plus **135**, 442 (2020).

[61] F. M. S. Lima, M. A. Amato, O. A. C. Nunes, A. L. A. Fonseca, B. G. Enders, and E. F. da Silva, Unexpected transition from single to double quantum well potential induced by intense laser fields in a semiconductor quantum well, J. Appl. Phys. **105**, 123111 (2009).

[62] E. J. Sie, *Coherent Light-Matter Interactions in Monolayer Transition-Metal Dichalcogenides* (Springer, Cambridge, 2017)

[63] A. Mysyrowicz, D. Hulin, A. Antonetti, A. Migus, W. T. Masselink, and H. Morkoc, "Dressed Excitons" in a Multiple-Quantum-Well Structure: Evidence for an Optical Stark Effect with Femtosecond Response Time, Phys. Rev. Lett. **56**, 2748 (1986).

[64] A. Muller, W. Fang, J. Lawall, and G. S. Solomon, Creating Polarization-Entangled Photon Pairs from a Semiconductor Quantum dot using the Optical Stark Effect, Phys. Rev. Lett. **103**, 217402 (2009).

[65] M. Gavrila and J. Z. Kaminski, Free-Free Transitions in Intense High-Frequency Laser Fields, Phys. Rev. Lett. **52**, 613 (1984).

[66] C. Pellegrini, A. Marinelli, and S. Reiche, The physics of x-ray free-electron lasers, Rev. Mod. Phys. **88**, 015006 (2016).

[67] H. Zimmermann, S. Meise, A. Khujakulov, A. Magaña, A. Saenz, and U. Eichmann, Limit on Excitation and Stabilization of Atoms in Intense Optical Laser Fields, Phys. Rev. Lett. **120**, 123202 (2018).

[68] M. Kübel, M. Spanner, Z. Dube, A. Y. Naumov, S. Chelkowski, A. D. Bandrauk, M. J. J. Vrakking, P. B. Corkum, D. M. Villeneuve, and A. Staudte, Probing multiphoton light-induced molecular potentials, Nat. Commun. **11**, 1 (2020).

[69] R. G. Mani, J. H. Smet, K. von Klitzing, V. Narayanamurti, W. B. Johnson, and V. Umansky, Zero-resistance states induced by electromagnetic-wave excitation in GaAs/AlGaAs heterostructures, Nature **420**, 646 (2002).

[70] W. A. Barletta, J. Bisognano, J. N. Corlett, P. Emma, Z. Huang, K. J. Kim, R. Lindberg, J. B. Murphy, G. R. Neil, D. C. Nguyen, C. Pellegrini, R. A. Rimmer, F. Sannibale, G. Stupakov, R. P. Walker, and A. A. Zholents, Free electron

lasers: Present status and future challenges, Nucl. Instrum. Methods Phys. Res., Sect. A **618**, 69 (2010).

[71] C. K. Choi, W. C. Henneberger, and F. C. Sanders, Intensity-dependent ionization potentials for H and He in intense laser beams, Phys. Rev. A **9**, 1895 (1974).

[72] J. I. Gersten and M. H. Mittleman, The shift of atomic states by laser fields, J. Phys. B **9**, 2561 (1976).

[73] C. A. S. Lima and L. C. M. Miranda, Hydrogen atom in superintense laser fields: Correction to the ground-state energy, Phys. Lett. A **86**, 367 (1981).

[74] F. Y. Qu, A. L. A. Fonseca, and O. A. C. Nunes, Intense laser field effect on confined hydrogenic impurities in quantum semiconductors, Phys. Status Solidi B **197**, 349 (1996).

[75] A. L. A. Fonseca, M. A. Amato, and O. A. C. Nunes, Intense field effects on impurities in semiconductors, Phys. Status Solidi B **186**, K57 (1994).

[76] In Ref. [61], the authors also reported another regime of unexpected transition of potential profiles from single to double wells under much stronger intense high-frequency laser fields. This case is not considered for this paper.

[77] S. Kim, J. Jin, Y. J. Kim, I. Y. Park, Y. Kim, and S. W. Kim, High-harmonic generation by resonant plasmon field enhancement, Nature **453**, 757 (2008).

[78] N. G. Asmar, A. G. Markelz, E. G. Gwinn, J. Černe, M. S. Sherwin, K. L. Campman, P. F. Hopkins, and A. C. Gossard, Resonant-energy relaxation of terahertz-driven two-dimensional electron gases, Phys. Rev. B **51**, 18041 (1995).

[79] N. H. Tolk, R. G. Albridge, A. V. Barnes, B. M. Barnes, J. L. Davidson, V. D. Gordon, G. Margaritondo, J. T. McKinley, G. A. Mensing, and J. Sturmann, Free-electron laser wavelength-selective materials alteration and photoexcitation spectroscopy, Appl. Surf. Sci. **106**, 205 (1996).

[80] R. Winkler, *Spin-Orbit Coupling Effects in Two-Dimensional Electron and Hole Systems* (Springer, New York, 2003).

[81] J. Y. Fu and J. C. Egues, Spin-orbit interaction in GaAs wells: From one to two subbands, Phys. Rev. B **91**, 075408 (2015).

[82] W. Wang, X. M. Li, and J. Y. Fu, Two distinct regimes for the electrical control of the spin-orbit interaction in GaAs wells, J. Magn. Magn. Mater. **411**, 84 (2016).

[83] See Supplemental Material at http://link.aps.org/supplemental/10.1103/PhysRevB.106.155420 for more details about formulations, constituent contributions of the confining potential for electrons, and the corresponding force fields, as well as the laser field control of spin-orbit coupling for an even narrower well of width equal to 10 nm.

[84] The bulk Rashba parameters are defined as follows [34]: $\eta_w = \frac{P^2}{3}(\frac{\delta_v/\delta_c}{E_g^2} - \frac{\delta_\Delta/\delta_c}{(E_g+\Delta)^2})$ and $\eta_H = -\frac{P^2}{3}(\frac{1}{E_g^2} - \frac{1}{(E_g+\Delta)^2})$, with P the Kane parameter, E_g the fundamental band gap, and Δ the split-off gap in the well layer. The parameters δ_c, δ_v, and δ_Δ stand for band offsets between the well and barrier layers, of the conduction band, heavy hole (and light hole), and split-off hole, respectively.

[85] By resorting to top and back gates (i.e., dual gate SO control) or to the interplay of gate and laser fields, one may achieve the SO manipulation while meanwhile locking the electron density to be fixed (i.e., constant density) as the gate (and laser) fields vary.

[86] For the case of single-subband occupation, this approximation is even better [34].

[87] T. Koga, J. Nitta, T. Akazaki, and H. Takayanagi, Rashba Spin-Orbit Coupling Probed by the Weak Antilocalization Analysis in InAlAs/InGaAs/InAlAs Quantum Wells as a Function of Quantum Well Asymmetry, Phys. Rev. Lett. **89**, 046801 (2002).

[88] T. Koga, Y. Sekine, and J. Nitta, Experimental realization of a ballistic spin interferometer based on the Rashba effect using a nanolithographically defined square loop array, Phys. Rev. B **74**, 041302 (2006).

[89] I. Vurgaftman, J. R. Meyer, and L. R. Ram-Mohan, Band parameters for III-V compound semiconductors and their alloys, J. Appl. Phys. **89**, 5815 (2001).

[90] H. Yang, Q. X. Wang, and J. Y. Fu, Interface involved Dresselhaus spin-orbit coupling in GaInAs/AlInAs heterostructures, Phys. Rev. B **104**, 125426 (2021).

[91] A. J. A. Beukman, F. K. de Vries, J. van Veen, R. Skolasinski, M. Wimmer, F. Qu, D. T. de Vries, B. M. Nguyen, W. Yi, A. A. Kiselev, M. Sokolich, M. J. Manfra, F. Nichele, C. M. Marcus, and L. P. Kouwenhoven, Spin-orbit interaction in a dual gated InAs/GaSb quantum well, Phys. Rev. B **96**, 241401(R) (2017).

[92] I. Knez, R. R. Du, and G. Sullivan, Evidence for Helical Edge Modes in Inverted InAs/GaSb Quantum Wells, Phys. Rev. Lett. **107**, 136603 (2011).

[93] E. Ozturk, H. Sari, and I. Sokmen, Electric field and intense laser field effects on the intersubband optical absorption in a graded quantum well, J. Phys. D: Appl. Phys. **38**, 935 (2005).

[94] B. McNeil and N. Thompson, X-ray free-electron lasers, Nat. Photonics **4**, 814 (2010).

[95] N. Picqué and T. W. Hänsch, Frequency comb spectroscopy, Nat. Photonics **13**, 146 (2019).

[96] Z. N. Chaleshtari, A. Haghighatzadeh, and A. Attarzadeh, Investigating the effect of position-dependent effective mass on the valence-band electronic states of GaAs/GaAsSb/GaAs parabolic quantum wells modulated by intense laser fields, Solid State Commun. **353**, 114870 (2022).

[97] The intersubband (c-c) energy separation for our GaInAs wells is about 100 meV, which is far smaller than the interband (c-v) one (i.e., band gap) of 816 meV [89]. Thus, the resonances of intersubband and interband transitions occur at about 25 and 200 THz, respectively. Thus, we consider a non-resonant laser field of, e.g., the frequency of about 100 THz (in between the two transitions but far exceeding the c-c resonance energy) or of more than 200 THz (exceeding both the c-c and c-v resonance energies).

[98] F. M. S. Lima, M. A. Amato, L. S. F. Olavo, O. A. C. Nunes, A. L. A. Fonseca, and E. F. da Silva, Intense laser field effects on the binding energy of impurities in semiconductors, Phys. Rev. B **75**, 073201 (2007).

[99] O. Madelung, *Group IV Elements and III-V Compounds* (Springer, New York, 1991).

[100] J. Beerens, G. Bernier, S. Lasserre, D. Pelenc, N. Puetz, and C. J. Miner, Magneto-optical study of $Ga_{0.47}In_{0.53}$ As-Inp under hydrostatic pressure, Can. J. Phys. **69**, 441 (1991).

[101] For a laser source with frequency ν (in terahertz) and output power I (in kW/cm^2), one can rewrite the laser parameter α_L in a more practical way with respect to ν and I, $\alpha_L \approx 7.31{\epsilon_r}^{-5/4}\sqrt{I}/\nu^2$ (in units of the effective Bohr radius α_B^*) [61,98]. For our GaInAs wells, we choose the high-frequency dielectric constant of $\epsilon_r = 11.7$ and the effective electron mass $m^* = 0.043m_0$ [89,99,100]. Then, for the range of laser pa-

rameter $\alpha_L = 0 - 7$ nm considered here, the corresponding maximum light intensity is about $2 \times 10^{11}\,\mathrm{W/cm^2}$ at $\nu = 100\,\mathrm{THz}$.

[102] H. Zimmermann, S. Patchkovskii, M. Ivanov, and U. Eichmann, Unified Time and Frequency Picture of Ultrafast Atomic Excitation in Strong Laser Fields, Phys. Rev. Lett. **118**, 013003 (2017).

[103] T. Ando, A. Iwasaki, and K. Yamanouchi, Strong-field Fourier Transform Vibrational Spectroscopy of d_2^+ using Few-Cycle Near-Infrared Laser Pulses, Phys. Rev. Lett. **120**, 263002 (2018).

[104] Z. R. Wei, J. L. Li, L. Wang, S. T. See, M. H. Jhon, Y. F. Zhang, F. Shi, M. H. Yang, and Z. H. Loh, Elucidating the origins of multimode vibrational coherences of polyatomic molecules induced by intense laser fields, Nat. Commun. **8**, 1 (2017).

[105] M. Fushitani, C.-N. Liu, A. Matsuda, T. Endo, Y. Toida, M. Nagasono, T. Togashi, M. Yabashi, T. Ishikawa, Y. Hikosaka, T. Morishita, and A. Hishikawa, Femtosecond two-photon Rabi oscillations in excited he driven by ultrashort intense laser fields, Nat. Photonics **10**, 102 (2016).

[106] A. Gonoskov, A. Bashinov, I. Gonoskov, C. Harvey, A. Ilderton, A. Kim, M. Marklund, G. Mourou, and A. Sergeev, Anomalous Radiative Trapping in Laser Fields of Extreme Intensity, Phys. Rev. Lett. **113**, 014801 (2014).

[107] S.-W. Bahk, P. Rousseau, T. A. Planchon, V. Chvykov, G. Kalintchenko, A. Maksimchuk, G. A. Mourou, and V. Yanovsky, Generation and characterization of the highest laser intensities ($10^{22}\,\mathrm{W/cm^2}$), Opt. Lett. **29**, 2837 (2004).

[108] For an even narrower well with an even stronger laser field, there may possibly emerge that both $\mathcal{E}_1$ and $\mathcal{E}_2$ are higher than $\mathcal{E}_c$. And, in this case, both β_1 and β_2 are expected to have strong dependence on the laser field.

[109] F. G. G. Hernandez, S. Ullah, G. J. Ferreira, N. M. Kawahala, G. M. Gusev, and A. K. Bakarov, Macroscopic transverse drift of long current-induced spin coherence in two-dimensional electron gases, Phys. Rev. B **94**, 045305 (2016).

[110] M. Luengo-Kovac, F. C. D. Moraes, G. J. Ferreira, A. S. L. Ribeiro, G. M. Gusev, A. K. Bakarov, V. Sih, and F. G. G. Hernandez, Gate control of the spin mobility through the modification of the spin-orbit interaction in two-dimensional systems, Phys. Rev. B **95**, 245315 (2017).

[111] R. Noguchi, K. Kuroda, K. Yaji, K. Kobayashi, M. Sakano, A. Harasawa, T. Kondo, F. Komori, and S. Shin, Direct mapping of spin and orbital entangled wave functions under interband spin-orbit coupling of giant Rashba spin-split surface states, Phys. Rev. B **95**, 041111(R) (2017).

[112] R. Song, N. Hao, and P. Zhang, Giant inverse Rashba-Edelstein effect: Application to monolayer $OsBi_2$, Phys. Rev. B **104**, 115433 (2021).

[113] M. Lee, M. O. Hachiya, E. Bernardes, J. C. Egues, and D. Loss, Spin Hall effect due to intersubband-induced spin-orbit interaction in symmetric quantum wells, Phys. Rev. B **80**, 155314 (2009).

[114] S. Souma, A. Sawada, H. Chen, Y. Sekine, M. Eto, and T. Koga, Spin Blocker using the Interband Rashba Effect in Symmetric Double Quantum Wells, Phys. Rev. Appl. **4**, 034010 (2015).

[115] E. Bernardes, J. Schliemann, M. Lee, J. C. Egues, and D. Loss, Spin-Orbit Interaction in Symmetric Wells with Two Subbands, Phys. Rev. Lett. **99**, 076603 (2007).

[116] P. Wojcik and J. Adamowski, Effect of inter- and intra-subband spin-orbit interactions on the operation of a spin transistor with a double quantum well structure, Semicond. Sci. Technol. **31**, 115012 (2016).

[117] J. Y. Fu, P. H. Penteado, D. R. Candido, G. J. Ferreira, D. P. Pires, E. Bernardes, and J. C. Egues, Spin-orbit coupling in wurtzite heterostructures, Phys. Rev. B **101**, 134416 (2020).